HIGH TEMPERATURE GAS KINETIC STUDY OF NITROUS OXIDE DECOMPOSITION PERFORMED WITH A SHOCK TUBE AND QUADRUPOLE MASS-FILTER

by
Daslin Guiman

May, 1965

Research Report No. 2

Research Group in Shock Tube Kinetics

R. L. Belford, Project Director

Noyes Chemical Laboratory
Department of Chemistry and Chemical Engineering
University of Illinois

U. S. Air Force Office of Scientific Research Grants
62-245 and 588-64

HIGH TEMPERATURE GAS KINETIC STUDY OF NITROUS OXIDE DECOMPOSITION PERFORMED WITH A SHOCK TUBE AND QUADRUPOLE MASS-FILTER

David Gutman, Ph.D.

Department of Chemistry

University of Illinois, 1965

A quadrupole mass-filter was built and coupled to a shock tube in order to study high temperature gas kinetics. The chemical kinetics of the decomposition of nitrous oxide was studied with this apparatus in order to establish the mechanism of the reaction at temperatures above 1000°K.

Several instrumentation problems unique to shock tube mass-spectrometry were solved. The most serious problem, that of a rapid-pumping ion source, was overcome by the design and construction of an unusually thin ion source.

The thermal decomposition of nitrous oxide was studied by shock-heating a mixture of 4% N_2O in argon and monitoring the ion currents corresponding to all of the principal species involved in the reaction: N_2O, N_2, O_2, NO, and O. In each run with the shock tube, the mass-filter was tuned to follow the concentration of a single species. Because enough runs were made with all of the species, a run for each species at the same temperature was made for several temperatures. The results of all of the experiments are listed below.

1. The mechanism of the N_2O decomposition between 1500°-2500°K is

(1a,b) $$N_2O + M \underset{k_{-1}}{\overset{k_1}{\rightleftarrows}} N_2O^* + M$$

(1c) $$N_2O^* \xrightarrow{k_u} N_2 + O$$

(2) $$O + N_2O \xrightarrow{k_2} N_2 + O_2$$

(3) $$O + N_2O \xrightarrow{k_3} 2NO$$

2. $k_3/k_2 = 1.2 \pm 0.2$ for all temperatures between 1500°-2500°K.

3. k_1 the second order rate constant for the thermal decomposition of N_2O in step 1 is equal to

$$k_1 = 1.2 \times 10^{-7} T^{1/2} \left(\frac{60{,}000 \text{ cal}}{RT}\right)^{5.09} e^{-\frac{60{,}000 \text{ cal}}{RT}} \frac{cc}{\text{mole sec}}$$

for the temperature range of 1500°-2500°K.

4. The observed steady state for O atoms, as well as the result that $k_3 \approx k_2$, confirms Fenimore's value for k_3 and shows that Kaufman's value for k_3 is inadequate.

ACKNOWLEDGMENT

I would like to express my gratitude first and foremost to Mr. Arthur J. Hay, a fellow graduate student whose manifold ideas and generous labors were essential to the success of this research. Mr. Hay was involved with this research almost from its inception, and worked diligently with both mind and body on the design and building of much of the experimental equipment. It is a pleasure to acknowledge his great help and to state that Mr. Hay's contribution was essential to the successful outcome of this research.

Secondly, I wish to thank my advisor, Professor R. L. Belford, for his guidance and encouragement. I especially wish to thank him for his understanding and patience with me during a series of troubled times.

Thirdly, it is a pleasure to acknowledge the help of the many people whose skill and interest were instrumental in the construction of the equipment: Stan Phillips and David Laker of the Chemistry Department Machine Shop, Benton Stevens and Fred Foltz of the Physical Plant Machine Shop, Jack Hughes and Harold Pope of the Physical Plant Tin Shop, Al Saldeen of the Chemistry Department Electronics Shop, and Nick Vasos of the Coordinated Science Laboratory.

Finally, I wish to thank the National Science Foundation, the Sun Oil Company, and the University of Illinois for the fellowships they awarded me.

TABLE OF CONTENTS

1 INTRODUCTION 1

1.1 SHOCK WAVE THEORY 1

1.2 THERMODYNAMIC PROPERTIES OF TEST GAS 3

1.3 SPECIAL CONSIDERATIONS BEHIND THE REFLECTED SHOCK WAVE 5

1.4 THE CHEMICAL PROBLEM: THE THERMAL DECOMPOSITION OF NITROUS OXIDE 7

1.4.1 BACKGROUND 7

2 EQUIPMENT 15

2.1 THE SHOCK TUBE 15

2.2 DIAPHRAGMS 17

2.3 GAS MIXING APPARATUS AND SHOCK TUBE VACUUM SYSTEM . . 24

2.4 SHOCK VELOCITY MEASUREMENT 30

2.5 THE QUADRUPOLE VACUUM SYSTEM 33

2.6 THE GAS ANALYSIS 34

2.6.1 THE ION SOURCE 37

2.6.2 THE QUADRUPOLE MASS FILTER 40

2.6.3 THE ION DETECTOR 44

3 EXPERIMENTAL 49

3.1 INTRODUCTION 49

3.2 CALIBRATION EXPERIMENTS 49

3.2.1 CALIBRATION EXPERIMENTS IN PURE ARGON 50

3.2.2 CALIBRATION EXPERIMENTS WITH NITROUS OXIDE 55

3.3 THE THERMAL DECOMPOSITION OF NITROUS OXIDE 56

3.3.1 THE MECHANISM OF NITROUS OXIDE DECOMPOSIGION . . . 56

3.3.2 THE RATE OF N_2O DECOMPOSITION 58

3.4 CONCLUSIONS 66

3.4.1 THE MECHANISM OF THE THERMAL DECOMPOSITION OF NITROUS OXIDE 66

3.4.2 THE STEADY STATE FOR OXYGEN ATOMS 67

3.4.3 THE RATE CONSTANTS k_2 AND k_3 68

3.4.4 THE RATE CONSTANT k_1 69

3.4.5 THE REACTION ABOVE 2500°K 74

BIBLIOGRAPHY 76

VITA 79

TABLE OF FIGURES

FIG. 1.1	SHOCK TUBE PERFORMANCE	2
FIG. 1.2	POTENTIAL ENERGY CURVES FOR N_2O DECOMPOSITION .	10
FIG. 2.1	GENERAL SCHEMATIC OF SHOCK TUBE AND VELOCITY MEASURING EQUIPMENT	18
FIG. 2.2	SHOCK TUBE PUMPING STATION	19
FIG. 2.3	DRIVER SECTION END OF SHOCK TUBE AND GAS HANDLING EQUIPMENT	20
FIG. 2.4	SHOCK VELICITY MEASURING STATIONS AND COUPLER TO HIGH VACUUM SYSTEM	21
FIG. 2.5	END FLANGE OF SHOCK TUBE SHOWING CONICAL LEAK INSERT AND THIN-FILM GAUGE INSERT	22
FIG. 2.6	DIAPHRAGM SCRIBING TOOL	25
FIG. 2.7	DIAPHRAGM SCRIBING TECHNIQUE	26
FIG. 2.8	GAS MIXING APPARATUS AND SHOCK TUBE VACUUM SYSTEM	28
FIG. 2.9	GAS STORAGE TANKS AND HIGH VACUUM MANIFOLD . .	29
FIG. 2.10	THIN-FILM RESISTANCE GAUGE MOUNTED ON SHOCK TUBE	32
FIG. 2.11	SCHEMATIC OF VACUUM SYSTEM HOUSING QUADRUPOLE MASS FILTER AND LAST SHOCK TUBE SECTION	35
FIG. 2.12	QUADRUPOLE VACUUM SYSTEM AND SHOCK TUBE	36
FIG. 2.13	THE ION SOURCE OF THE QUADRUPOLE MASS FILTER AND SHOCK TUBE END SECTION	41
FIG. 2.14	ELECTRON MULTIPLIER FOR DETECTING ION CURRENT .	47
FIG. 2.15	ELECTRON MULTIPLIER AND DEFLECTION LENS FOR ION CURRENT DETECTION	48
FIG. 3.1	EXPERIMENTAL ARGON ION SIGNAL CURVES	54
FIG. 3.2	A SAMPLE OF PLOTS FOR CALCULATING PSEUDO FIRST ORDER DECOMPOSITION RATE CONSTANT OF N_2O. RUN NO. F206513, T = 2528°K.	61

TABLE OF FIGURES (continued)

FIG. 3.3 ION CURRENT CURVES IN NITROUS OXIDE DECOMPOSITION REACTION 62

FIG. 3.4 THERMAL DECOMPOSITION RATE OF N_2O (ALL EXPERIMENTS) 63

FIG. 3.5 THERMAL DECOMPOSITION RATE OF N_2O (ALL EXPERIMENTS BELOW 2500°K) 64

FIG. 3.6 JOST ET AL'S DATA ON THERMAL DECOMPOSITION OF N_2O 73

TABLE OF TABLES

TABLE 2.1 ION SOURCE VOLTAGES ON QUADRUPOLE MASS-FILTER . . . 42

TABLE 3.1 PRESSURE DEPENDENCE TESTS 55

TABLE 3.2 EXPERIMENTAL DATA ON 41 SHOCK TUBE EXPERIMENTS DONE WITH 4 PER CENT N_2O IN ARGON 59

1 INTRODUCTION

1.1 SHOCK WAVE THEORY

The shock tube is now a well-established and effective tool for the study of high temperature chemical kinetics. The theory of shock waves and their applications in the fields of chemistry and physics have been covered in four books,[1-4] several review articles,[5-9] and more than 200 research articles. Therefore, the basic theory will not be elaborated on in this paper. A brief outline is given below, with special emphasis on those aspects most important to this study.

The shock tube consists of a tube of constant cross-section, which is divided into a driver section and a test section (Figure 1.1). The two parts are separated by a thin metal diaphragm. The gas to be studied (usually highly diluted in an inert gas) is admitted into the test section to a final pressure of 2-10 mm Hg (Region 1). Then a driver gas, usually helium, is admitted into the driver section (Region 4) until the pressure forces the diaphragm to burst. This causes a shock wave to move out into the test gas. The shock wave moves through the test gas (Region 1) and heats it (Region 2). The shock wave is followed by the contact surface, which is the boundary between the test gas and the driver gas. Region 3 is the expanded driver gas which is moving down the tube. When the shock wave arrives at the end of the tube A, it reflects back up the tube. The reflected shock wave is caused by the gas coming to rest at the end of the tube. The kinetic energy of motion of the gas behind the incident wave is converted to heat as the gas comes to rest, so that region behind the

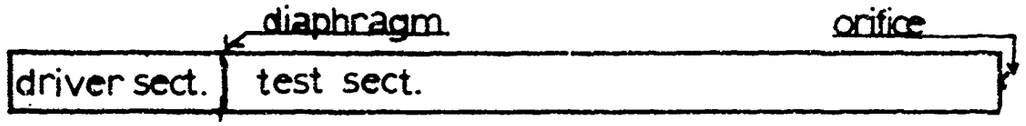

(a.) shock tube

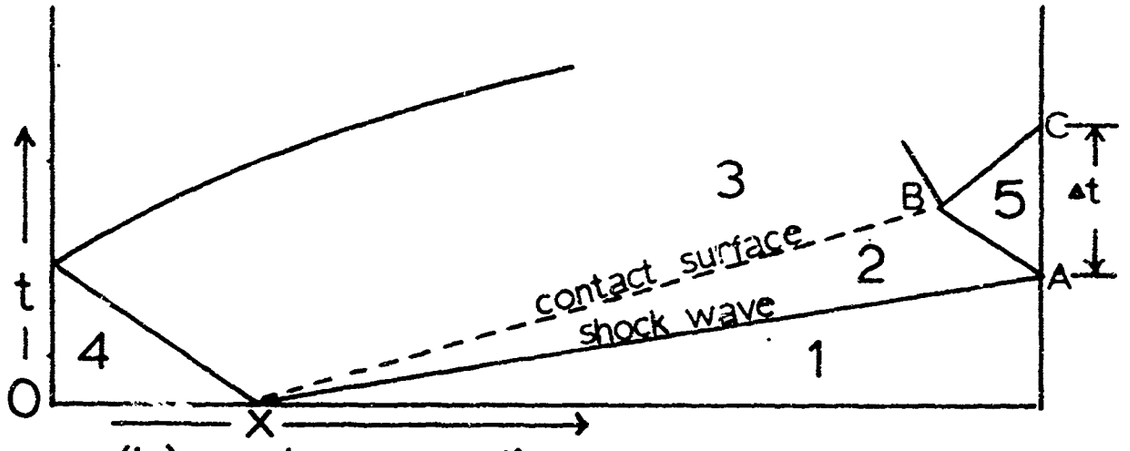

(b.) x–t wave diagram

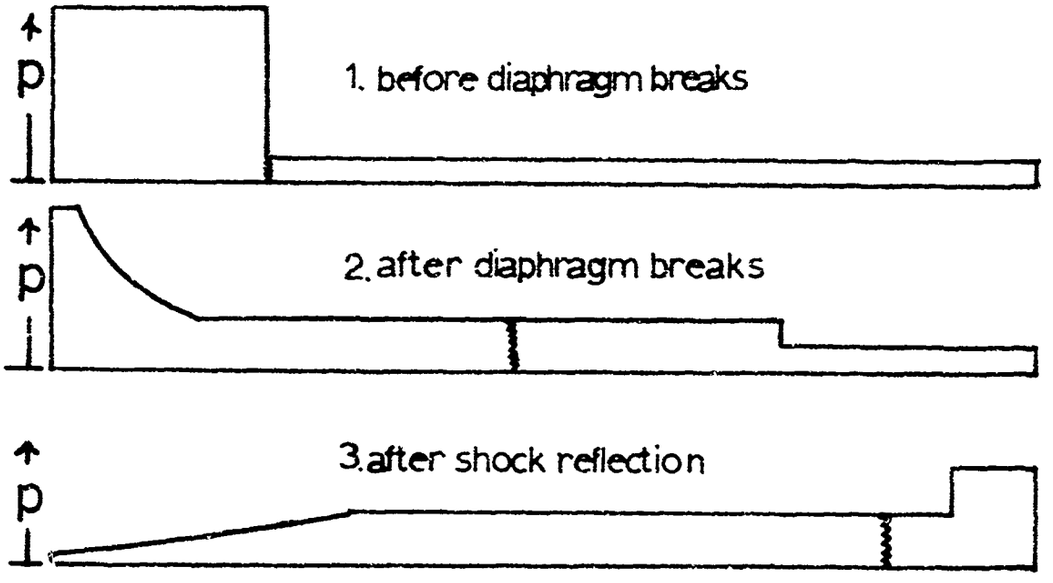

(c.) shock tube pressure profiles

FIG. 1. SHOCK TUBE PERFORMANCE

reflected shock wave (Region 5) consists of gas which is at rest and which is heated to a temperature approximately twice that of Region 2. The reflected shock wave soon interacts with the contact surface B and then returns to the end wall C. In the time interval Δt between A anc C the gas at the end of the tube is uniformly heated and remains at this high temperature until the reflected shock wave returns at C. This time interval is on the order of one millisecond.

A small orifice in the end of the tube permits a continuous stream of test gas to flow out of the tube directly into the ion source of a mass-spectrometer, where it is analyzed.

1.2 THERMODYNAMIC PROPERTIES OF TEST GAS

The shock wave that moves through the test gas heats it, raises its pressure, and sets it into uniform motion down the tube. The properties of the gas behind the shock wave are found by solving the three conservation equations: one for mass, one for momentum, and one for energy. When a coordinate system which moves with the shock wave is used, the flow becomes steady and all the conservation equations are independent of time. We assume that the flow is adiabatic in the time intervals of interest and that the gas flow is nonviscous. With these assumptions and the moving coordinate system, the equations are

$$\rho_1 u_1 = \rho_2 u_2 \quad , \qquad \text{(Mass Conservation)}$$

$$\rho_1 u_1^2 + p_1 = \rho_2 u_2^2 + p_2 \quad , \qquad \text{(Momentum Conservation)}$$

$$\frac{1}{2}u_1^2 + h_1 = \frac{1}{2}u_2^2 + h_2 \quad , \qquad \text{(Energy Conservation)}$$

where ρ = density, u = particle velocity, p = pressure, h = enthalpy per gram. The subscript 1 refers to region 1, the unshocked gas, and the

subscript 2 refers to the heated gas behind the incident shock wave. The unshocked gas has a velocity, u_1, equal in magnitude but opposite in sign to the velocity of the shock wave, because the coordinate system moves with the shock front.

Two more equations are needed to solve for all the unknowns. The equation of state of the gas is taken to be that of an ideal gas. The ideal gas law is well-obeyed, because the test gas is usually 96% argon at low pressure and at high temperature. The form of the law which is used is

$$p = \rho RT$$

where T = absolute temperature and R = the gas constant per gram. The other equation relates the enthalpy of the gas to temperature. Since we are assuming our gas is ideal, the enthalpy is only a function of temperature and may be written

$$h = h^{o}(T) \ .$$

The specific form of the equation depends on the gas mixture under consideration.

The eight variables can be reduced to five by giving the initial conditions before the shock is fired, p_1 and T_1, and by measuring the speed of the shock wave, which is $-u_1$. This then leaves five unknowns, which can be determined from the five equations.

A similar argument applies to the reflected shock wave. In this case, however, the reflected shock velocity need not be measured because of the additional constraint that all gas must come to rest at the end of the tube.

Because the enthalpy is usually expressed as a power series in T, the equations cannot be solved explicitly for the variables. However, it is a simple problem for the computer to solve these equations by an iterative technique, which guesses a final temperature and then calculates a better one, until the two values agree to within the desired accuracy. Dr. Roger Strehlow and Harry Dyner of the Aeronautical Engineering Department, University of Illinois, have written such a program for their own use. They kindly ran off tables giving all the variables as a function of shock velocity for the test gas we studied. The variables were listed as dimensionless ratios which could be solved for the final temperature, pressure, and density by using the corresponding initial conditions. A discussion of such a program has been given by Bird, Duff and Schott.[10]

1.3 SPECIAL CONSIDERATIONS BEHIND THE REFLECTED SHOCK WAVE

As was previously mentioned, the final temperature and pressure behind the reflected shock wave were calculated assuming the flow was nonviscous and adiabatic. Because the reflected shock wave moves back through the oncoming heated test gas, its flow will not be ideal if a boundary layer has developed behind the incident shock wave. This problem has been studied by Skinner,[11] Rudinger,[12] and others, and has recently been reviewed by Johnson and Britton.[13] Johnson and Britton concluded that the actual temperature behind the reflected shock wave is probably about $35^{\circ} \pm 5^{\circ}$ lower than that calculated by assuming nonviscous flow. They give this estimate for the temperature range 1500°-1900°K. However, they also concluded that the temperature at the back wall of the tube would correspond to the ideal value, because the gas is twice heated at the same instant; hence, there has been no time for a boundary layer to

develop. Since this is the area in which we sample our gas, the nonideality due to viscous flow is unimportant.

A more serious problem is the cooling of the gas being sampled from the orifice, caused by the end plate of the shock tube. Bradley and Kistiakowsky[14] have discussed the problem qualitatively and Dove and Moulton[15] have done some rough reasoning based on some calculations by Skinner.[16] Since the boundary layer is constantly growing, the problem is non-steady and solution is very difficult. Dove and Moulten have assumed a steady model, which they feel should give rough values for the effect. They use as their criteria for serious distortion of the kinetic results a temperature drop of 10% in the gas being sampled. They concluded that at 1500°K the effect of cooling at the end wall should be serious after 1.4 milliseconds. Dove and Moulten conclude, however, that the whole problem must undergo experimental testing in order to determine the true quantitative effect.

The experiments reported in this paper give a similar qualitative picture. All data were evaluated by extrapolating the rate constants to the time of shock arrival. The fact that all the rate constants decreased with time shows that cooling is an effect which does occur, and which becomes worse as the time increases. One difficulty in using the data in this paper to calculate the magnitude of this effect is that there is no quantitative data on the nitrous oxide decomposition above 2500°K done by an independent method. There would have to be a comparison with an independent study in order to give a quantitative basis to this effect. Below 2500°K the agreement with other experiments is good and hence we conclude that the experimental method yields good quantitative data up to this temperature, if the rate data is extrapolated to the time of shock arrival.

Several other chemical studies have been made in which a shock tube was coupled to a time-of-flight mass-spectrometer.[14-20] The sampling technique was similar. The time-of-flight spectrometer is a rapid-scanning instrument and sacrifices accuracy for speed. Therefore, all these studies have been semi-quantitative. Within their range of accuracy, the experimental results have been consistent with the temperature calculated from the ideal theory. In the study of the dissociation rate of chlorine by R. W. Diesen,[19] he finds a fall-off in the rate constant from the theoretical value above 2500°K. He has good agreement below this temperature. He suggests that this fall-off might originate in a depopulating of the higher vibrational states, causing the rate constant to rise more slowly with temperature than one would expect from collision theory. However, the effect is in the same direction as the cooling effect would be. We have found that in the nitrous oxide experiments the points also fall away from a reasonable simple theoretical curve about 2500°K. Therefore, until further evidence is available for the higher temperatures, we shall assume 2500°K to be the safe upper limit for good quantitative results by shock tube mass-spectrometry.

1.4. THE CHEMICAL PROBLEM: THE THERMAL DECOMPOSITION OF NITROUS OXIDE

1.4.1 BACKGROUND

The thermal decomposition reaction of nitrous oxide has always been of great interest because it is one of the simplest molecules capable of undergoing unimolecular decomposition, since it is both linear and triatomic. The entire unimolecular fall-off region is experimentally accessible, making N_2O a useful molecule with which to test various unimolecular theories.

Unfortunately, the thermal decomposition is not simple and care must be taken in interpreting the experimental data. Johnston[21] (1951) has reviewed all the work done on this reaction prior to 1950. Before this time, activation energies ranging from 48 to 65 kcal per mole had been reported and the data did not fit any existing theories. Johnston assumed a simple model for the reaction, which is given below.

(1) $N_2O + N_2O \longrightarrow N_2O^* + N_2O$

(2) $N_2O + N_2O^* \longrightarrow N_2O + N_2O$

(3) $N_2O^* \longrightarrow N_2 + O$

(4) Recombination of oxygen atoms on the wall

(5) Recombination of oxygen atoms by three body collisions

Thus, he assumed that the reaction is predominantly a simple unimolecular decomposition followed by secondary side reactions which do not activate or consume much nitrous oxide. By extrapolating all first order rate constants to zero concentration, Johnston obtained residual constants which he attributed to the heterogeneous reactions, and he subtracted these constants from the corresponding first order constant at the same temperature. After this he fitted all data points at the same pressure to a curve in the form $\log k = \log A - E/2.303RT$ and evaluated the constant at 888°K. Now a plot of all these points, log k versus log (N_2O), gave a smooth, continuous curve. The graph showed that the low pressure limit at 888°K corresponded to a density of 0.01×10^{-4} moles/cc and that the high pressure limit was never reached, even at 5×10^{-4} moles/cc--the upper limit of the study. At the low pressure limit, Johnston calculated the activation energy to be 59 kcal/mole, which gave a

normal pre-exponential factor and "number of oscillators". In the fall-off region the agreement with theories was not very good.

Subsequent attempts to correlate old data with new theories were made but resulted in only limited success.[22-25]

There is another problem which makes theoretical comparisons difficult. The measured activation energy of N_2O decomposition is less than 84.7 kcal/mole, the dissociation energy of the ground state (Figure 1.2). This has been explained by Stearn and Eyring[26] as due to predissociation along either the $^3\Sigma$ or $^3\Pi$ state of nitrous oxide. They calculated that the activation energy could be as low as 52 kcal/mole. Using the experimental activation energy of Nagasako and Volmer,[27] 53 kcal/mole, Stearn and Eyring calculated a transmission coefficient $\kappa = 1.88 \times 10^{-4}$. Gill and Laidler[25] point out that with the higher activation energy, which is now regarded as more likely, κ is on the order of 10^{-1} to 10^{-2}.

The simple mechanism used by Johnston[21] was not sufficient to explain the experimental facts. As early as 1926, Briner, Meiner and Rothen[28] presented results showing NO formed as a product in the nitrous oxide decomposition. Later work by Musgrave and Hinshelwood[28] (1932) revealed that: (1) Considerable NO was produced during the early stages of the reaction; (2) It was not destroyed later; and (3) It inhibited its further production. They concluded that the mechanism must include the following steps:

(1) $$N_2O \longrightarrow N_2 + O$$

(2) $$O + N_2O \longrightarrow 2NO$$

(3) $$NO + O + M \longrightarrow NO_2 + M$$

Pease[30] (1939) later proposed a chain reaction which required the initial step to be:

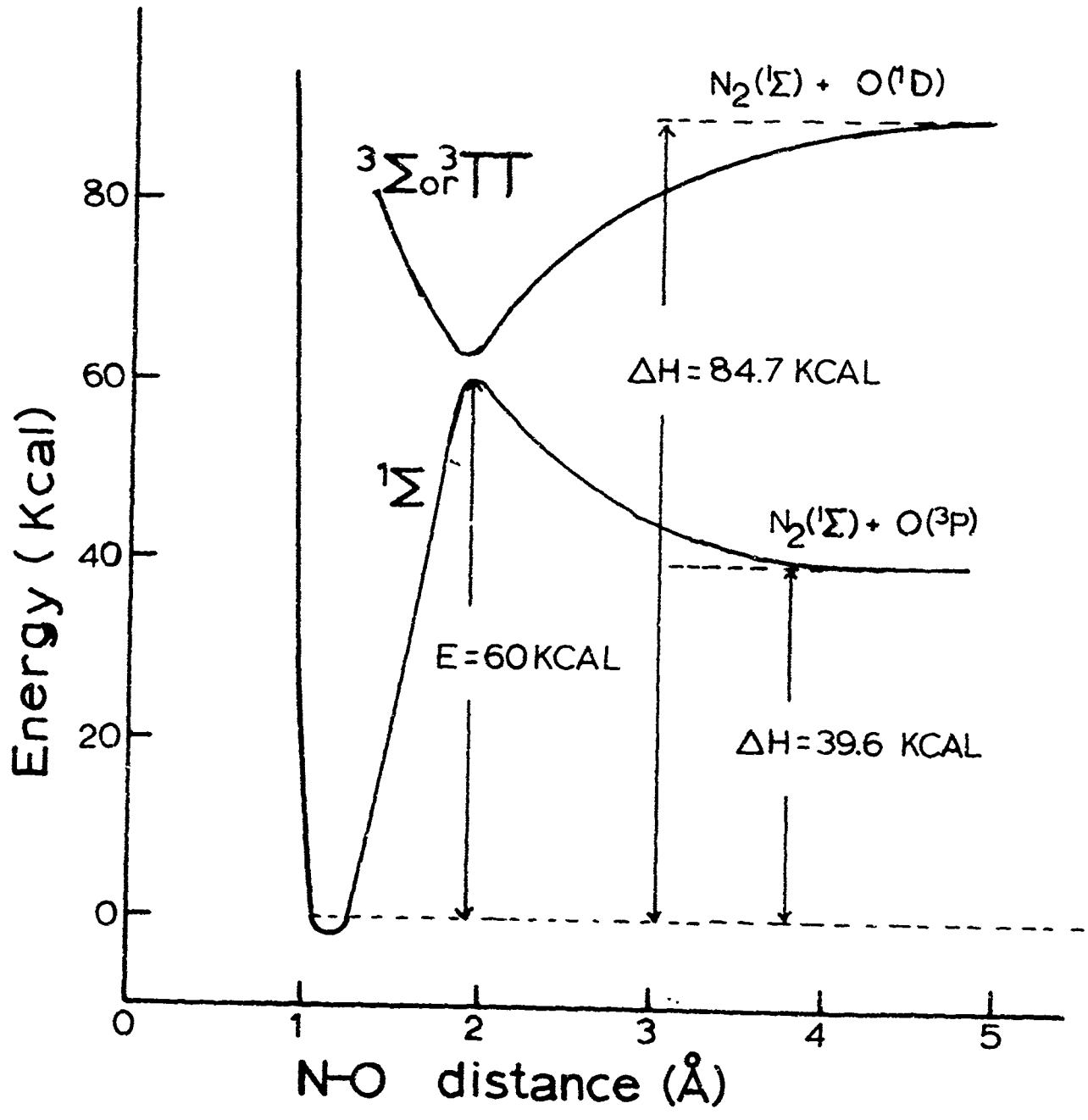

FIG. 1.2 POTENTIAL ENERGY CURVES FOR N_2O DECOMPOSITION

(1) $N_2O \longrightarrow NO + N$

This step is energetically prohibitive (ΔH_0^o = +113 kcal) and was rigorously ruled out by N^{15} tracer experiments done by Friedman and Bigeleisen[31] (1953).

Kaufman, Gerri, and Bowman[32] (1956) studied the thermal decomposition of N_2O in a quartz vessel which could be heated to about 1000°K. They monitored both the N_2O and the NO concentration as a function of time. They proposed the following mechanism, which explained most of their results:

(1) $N_2O \xrightarrow{k_1} N_2 + O$ $\quad \Delta H_0^o = +38.3$ Kcal

(2) $O + N_2O \xrightarrow{k_2} N_2 + O_2$ $\quad \Delta H_0^o = -78.9$ Kcal

(3) $O + N_2O \xrightarrow{k_3} 2NO$ $\quad \Delta H_0^o = -35.9$ Kcal

(4) $O + NO + M \xrightarrow{k_4} NO_2 + M$ $\quad \Delta H_0^o = -71.4$ Kcal

(5) $O \xrightarrow{k_5}$ Wall

(6) $NO_2 + N_2O \xrightarrow{k_6} N_2 + O_2 + NO$ $\quad \Delta H_0^o = -7.5$ Kcal

The reaction $O + O + M \rightarrow O_2 + M$ was not included because of the low probability for such triple collisions. Reaction 6 was included to show that any NO formed in 3 would not be destroyed, but still may deplete oxygen atoms by 4, only to be regenerated by 6. On the basis of this mechanism, Kaufman gives

$$k_2 = 3 \times 10^{10}\, e^{-14{,}500 \text{ cal/RT}} \ \frac{cc}{\text{mole sec}}$$

$$k_3 = 1 \times 10^{11}\, e^{-15{,}500 \text{ cal/RT}} \ \frac{cc}{\text{mole sec}}$$

Fenimore and Jones[33] (1958) studied reaction 3 by introducing N_2O gas into a flame in which the O atom concentration could be calculated. They assumed the only source of NO was reaction 3 and found

$$k_3 = 2 \times 10^{14} e^{-32,000 \text{ cal/RT}} \frac{\text{cc}}{\text{mole sec}}$$

Later work by Fenimore and Jones[34] (1962) modified this value slightly to give

$$k_3 = 1 \times 10^{14} e^{-28,000 \text{ cal/RT}} \frac{\text{cc}}{\text{mole sec}}$$

(We quote a value which is one-half that actually given in the paper by Fenimore and Jones,[34] who reported the constant based on the rate of NO formation. We define k_3 as the rate constant for the disappearance of O atoms; our convention is also the one used by Kaufman et al..[32])

The difference between Kaufman et al.'s value for E_3 = 15.5 kcal/mole and Fenimore and Jones's value E_3 = 28 kcal/mole has been the subject of considerable literature. Fenimore and Jones's value has been questioned not only by Kaufman and co-workers, but also by Reuben and Linnett[35] (1959) and Bradley and Kistiakowsky[14] (1961). Reuben and Linnett reinterpreted the results of Kaufman, et al. They proposed a mechanism in which the O atoms in the decomposing nitrous oxide were "hot" atoms possessing about 12 kcal excess translational energy which would react preferentially via reaction 3; but after a few nonreactive collisions, these O atoms would lose their excess energy and no longer react via 3. They claimed that their results confirmed Kaufman's value for E_2.

Bradley and Kistiakowsky,[14] using a shock tube coupled to a time-of-flight mass spectrometer, studied the high temperature decomposition of N_2O and concluded that their experimental results could only be explained using Kaufman's value for k_3 and thus disproved Fenimore's value for E_3.

Fenimore successfully defended himself from all three sides. In a short communication,[36] Fenimore showed that the results of Bradley and Kistiakowsky did not disprove his value for k_3 and that their results were not even self-consistent. In an earlier paper[33] (1958), Fenimore and Jones point out that Kaufman's lower E_3 comes from assuming no temperature dependence for the loss of O atoms on the wall. Also, Kaufman's E_3 forces reaction 4 to have a negative activation energy of 11 kcal. Had Kaufman's E_3 been 11 kcal higher (26.5 kcal), reaction 4 would have zero activation energy, which would be more reasonable for that reaction. Fenimore and Jones[34] dispose of Reuben and Linnett's hypothesis by showing that their theory leads to an impossible situation. If E_3 were 15 kcal/mole, the pre-exponential factor would have to be lower--about 10^{-3} of the collision frequency--and the "hot" atom would have ample time to "cool off" before reaction. Hence, no NO should form by their mechanism.

Kaufman has reconsidered his value,[37] and on the basis of more recent experiments[38] he has arrived at a new value for E_3--21 kcal/mole. He admits this value is probably quite inaccurate and that more work needs to be done.

Fenimore and Jones[34] point out that their value for k_3 is confirmed by an entirely different argument. If their value for k_3 is combined with the experimental rate constant for the reverse reaction (the thermal decomposition of NO) as determined by Kaufman and Kelso,[39] it results in exactly the thermodynamic value of the equilibrium constant for the reaction

$$N_2O + O \rightleftarrows 2NO$$

Two recent shock tube studies indirectly confirm Fenimore's value. Jost, Michel, Troe and Wagner[40] (1964) studied the thermal decomposition

of nitrous oxide in a shock tube. They monitored the ultraviolet absorption of N_2O and NO. Since the N_2O continuum overlapped the band spectrum of NO, the NO absorption was only used after all the N_2O had decomposed. Besides obtaining a value for k_1, they indirectly confirmed Fenimore and Jones's value by finding that at all temperatures between 1500°-2500°K a quasi steady-state existed with respect to O atoms. Kaufman's E_3 is too low to make k_3 sufficiently large to insure a steady state up to 2500°K. Jost et al. also observed that in the entire range 1500-2500°K the residual NO concentration was the same. This actually is in accord with our finding, that $k_2 \approx k_3$, which is reported in Section 3.

Fishburne and Edse[41] also studied the thermal decomposition of N_2O in a shock tube and determined various values for k_1 and E_1 as functions of pressure. They ignored subsequent reactions, such as 2 and 3, because they claimed they were too slow. The work of Jost and co-workers and the experiments reported in Section 3 of this paper show that steps 2 and 3 should have been given more serious consideration.

If we call k_1' the experimentally determined second order rate constant for the decomposition of N_2O, the value for k_1' as determined by Jost et al. is

$$k_1' = 10^{15.3} \times e^{-61,000 \text{ cal/RT}} \frac{\text{cc}}{\text{mole sec}}$$

and the value found by Fishburne and Edse is

$$k_1' = 9.65 \times 10^{13} e^{-49,500 \text{ cal/RT}} \frac{\text{cc}}{\text{mole sec}}$$

Fishburne and Edse[41] report first order rate constants and the above rate constant was obtained by dividing their constant by the reported density, 0.13×10^{-4} moles/cc.

2 EQUIPMENT

2.1 THE SHOCK TUBE

The overall length of the shock tube is twenty feet. It is divided into a sixteen-foot test section and a four-foot driver section (Figure 2.1). It is made in five flanged sections. Four are made from schedule 80 (2.900 inches I.D., 0.300 inches wall thickness) 316 stainless steel pipe, and one is made from three-inch I.D. Pyrex brand double tough glass pipe. A gradual taper is cut into the two ends of stainless steel pipe joining the glass section to give a smooth inside wall. The sections are numbered in Figure 2.1.

Section 1, the driver section, is four feet long. It has a pumping port (Figure 2.2) to evacuate it between runs and a gas inlet valve to admit the driver gas. The entire section sits on rollers that allow one to slide it back between runs in order to replace the metal diaphragm between Sections 1 and 2. The photograph, Figure 2.3, shows the driver section with its pumping port to the extreme right. In the background is the gas handling equipment for both the driver section and the test section, to be described in section 2.3.

Both sections one and two have identical pumping ports (Figure 2.2). The valve seat is made from stainless steel, and the side exposed to the shock tube is radiused so that when the valve is closed, the inside wall has no discontinuities. This gives smooth flow past these ports when the shock wave passes. The bellows assembly is from a one-inch Veeco Type R high-vacuum-sealed valve. All the other parts were designed and machined

for this application. The valve has excellent conductance for initial pumping-down of the shock tube and with its o-ring seals gives no measurable leaks when tested with a helium mass spectrometer leak detector.

Section 2 is two and one-half feet long. As mentioned above, it has an identical pumping port (Figure 2.2) to evacuate the test section between runs. This section also has a gas inlet valve to admit the gas to be tested. All the sections from numbers 2 to 5 constitute the test section and are filled with the test gas from this valve. Figure 2.3 shows part of the test section visible in the laboratory. The lighter section is the only section made from glass.

Section 3 is ten feet long. It is made from glass because of its low initial cost and ease in cleaning. The light color of the section comes from a fiberglass epoxy casing surrounding the pipe to protect against flying glass in the event of breakage.

Section 4 is two and one-half feet long and has four velocity measuring stations to be described in 2.5.

Section 5, the last section, is one foot long. It is coupled to the vacuum chamber containing the quadrupole mass filter. The coupler can be seen in Figure 2.4 together with the velocity measuring stations.

A plate on the end of the section contains a small conical or hyperbolic orifice, which allows gas from the shock tube to flow directly into the ion source of the mass filter (Figure 2.5). An o-ring in the end of the shock tube makes a gas-tight seal with the plate, and 10 bolts hold the plate firmly against the end of the shock tube.

The leak is in the center of a small disk 0.400 inches in diameter and 0.020 inches thick, which is in turn brazed into the larger end plate. The hole in the center of the plate is shouldered so that when the disk is

in place there is again an even surface. The leak is 0.002 inches in diameter on the inside of the plate. It keeps this dimension for about 0.001 inches and then breaks out into a 60° cone for the remaining 0.019 inch thickness of the disk. The disks with the leaks are obtained from the Spinnerette Department, Baker Platinum Division of Engelhard Industries, Inc.

In the same end plate is another hole, which supports a thin-film resistance gauge exactly the same as those used to detect the passage of the shock wave. They are described in Section 2.4. As with the disk containing the lead, this gauge is flush mounted so that the inside surface of the end plate of the shock tube is free from recesses or protrusions.

2.2 DIAPHRAGMS

The diaphragms which separate the driver gas from the test gas are placed between Sections 1 and 2. After the gas being studied has been admitted to the test section, gas is admitted to the driver section until the diaphragm bursts.

Early in the development of this project it was decided not to use organic diaphragm materials, which would introduce organic debris into the shock tube with the firing of every shock. This would have necessitated frequent cleaning of the shock tube to remove impurities. Several thicknesses of aluminum foil were tried as diaphragm material, but invariably pieces of this thin foil were torn away and carried down the tube with each shock. Thicker pieces of aluminum foil were tried, but the high pressures required to rupture the diaphragm produced very strong shocks and, therefore, temperatures higher than desired.

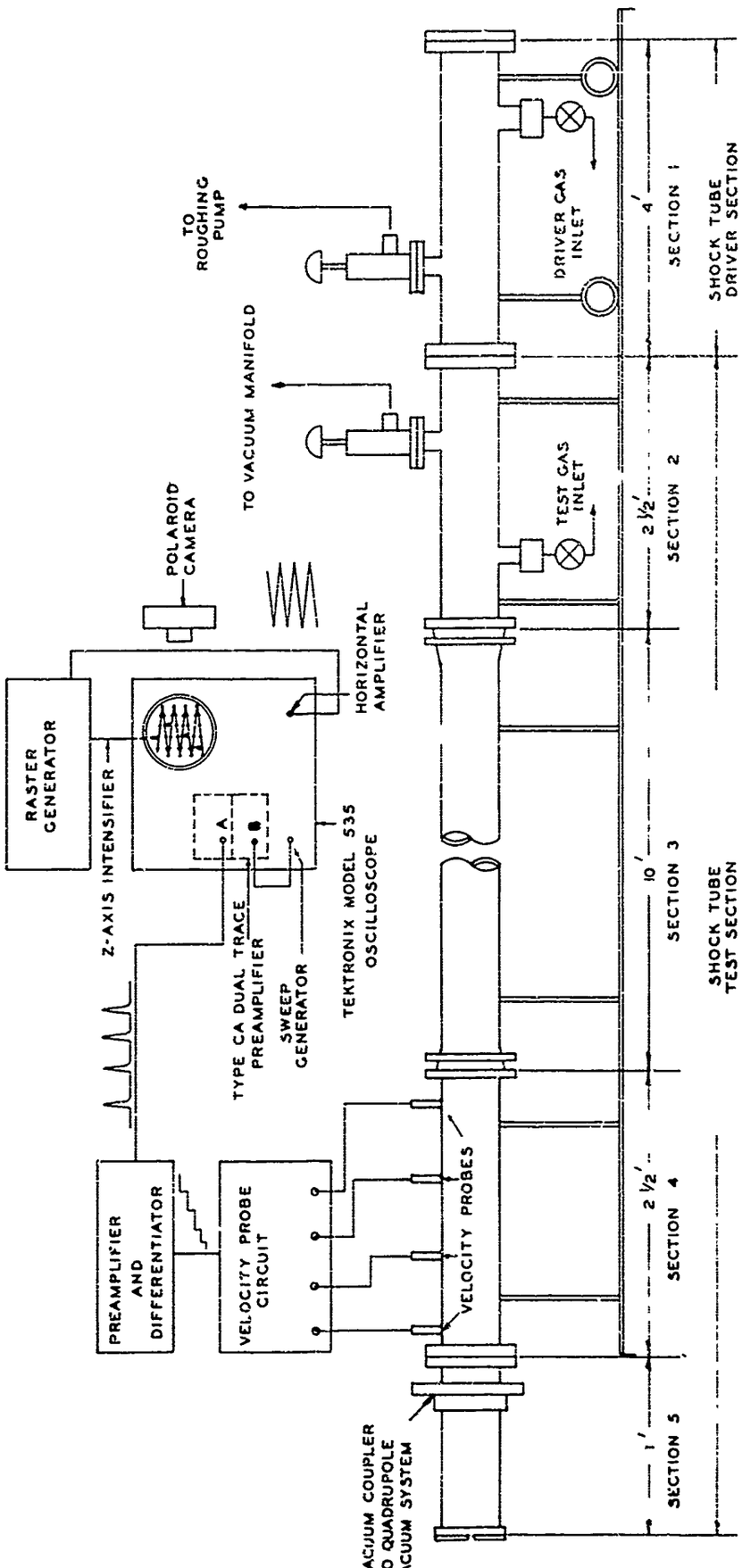

FIG. 2.1 GENERAL SCHEMATIC OF SHOCK TUBE AND VELOCITY MEASURING EQUIPMENT

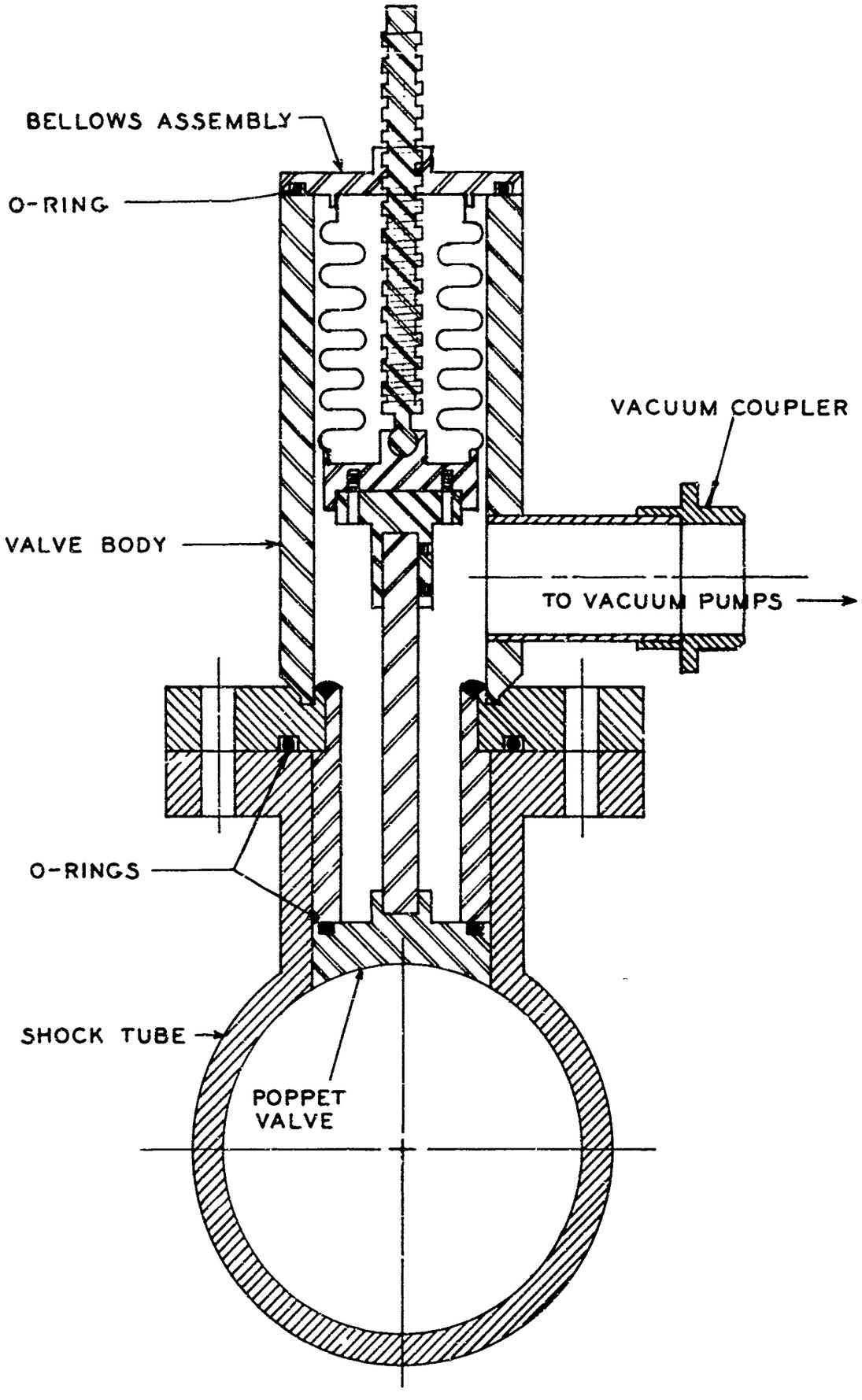

FIG. 2.2 SHOCK TUBE PUMPING STATION

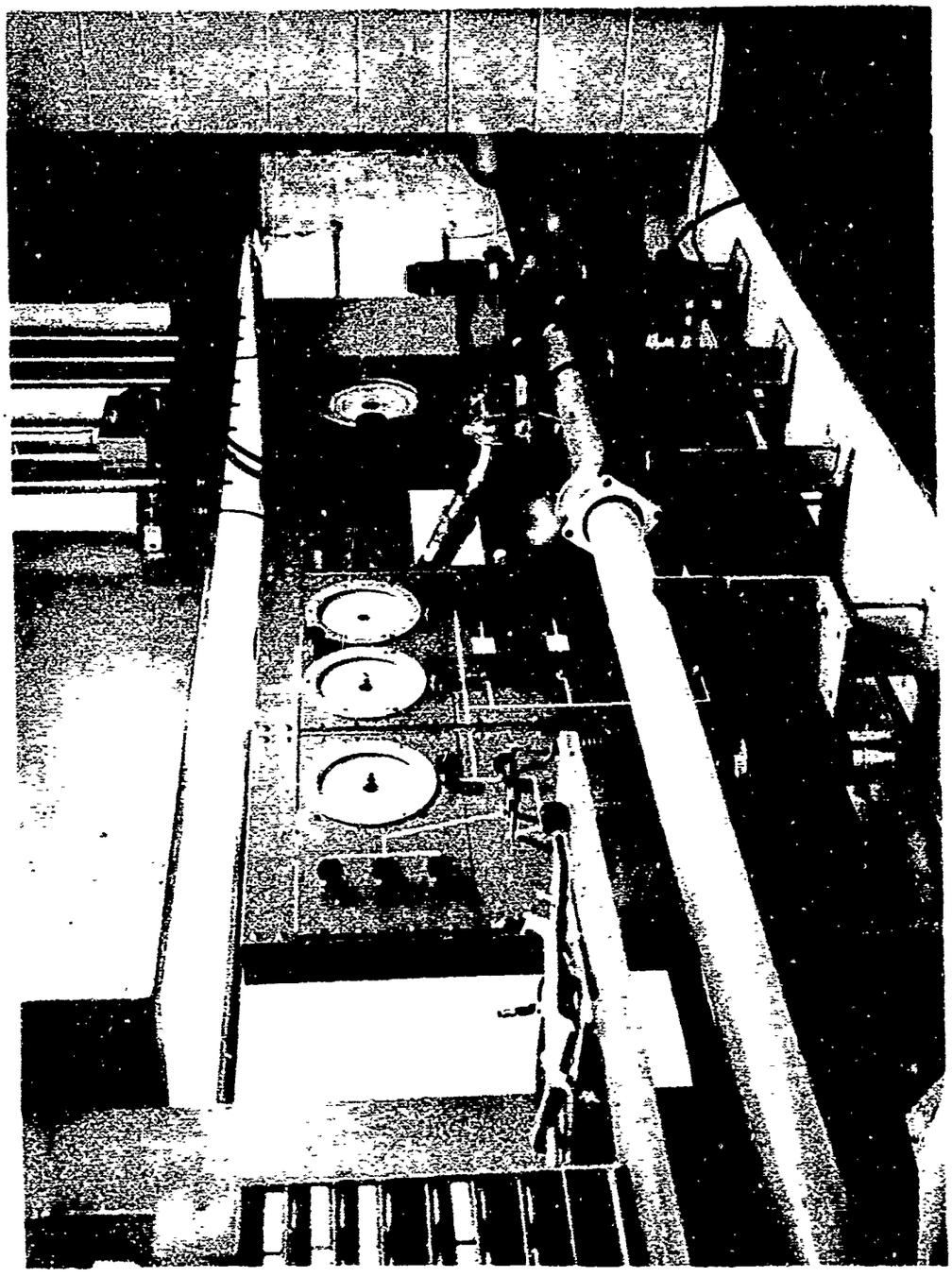

FIG. 2.3 DRIVER SECTION END OF SHOCK TUBE AND GAS HANDLING EQUIPMENT

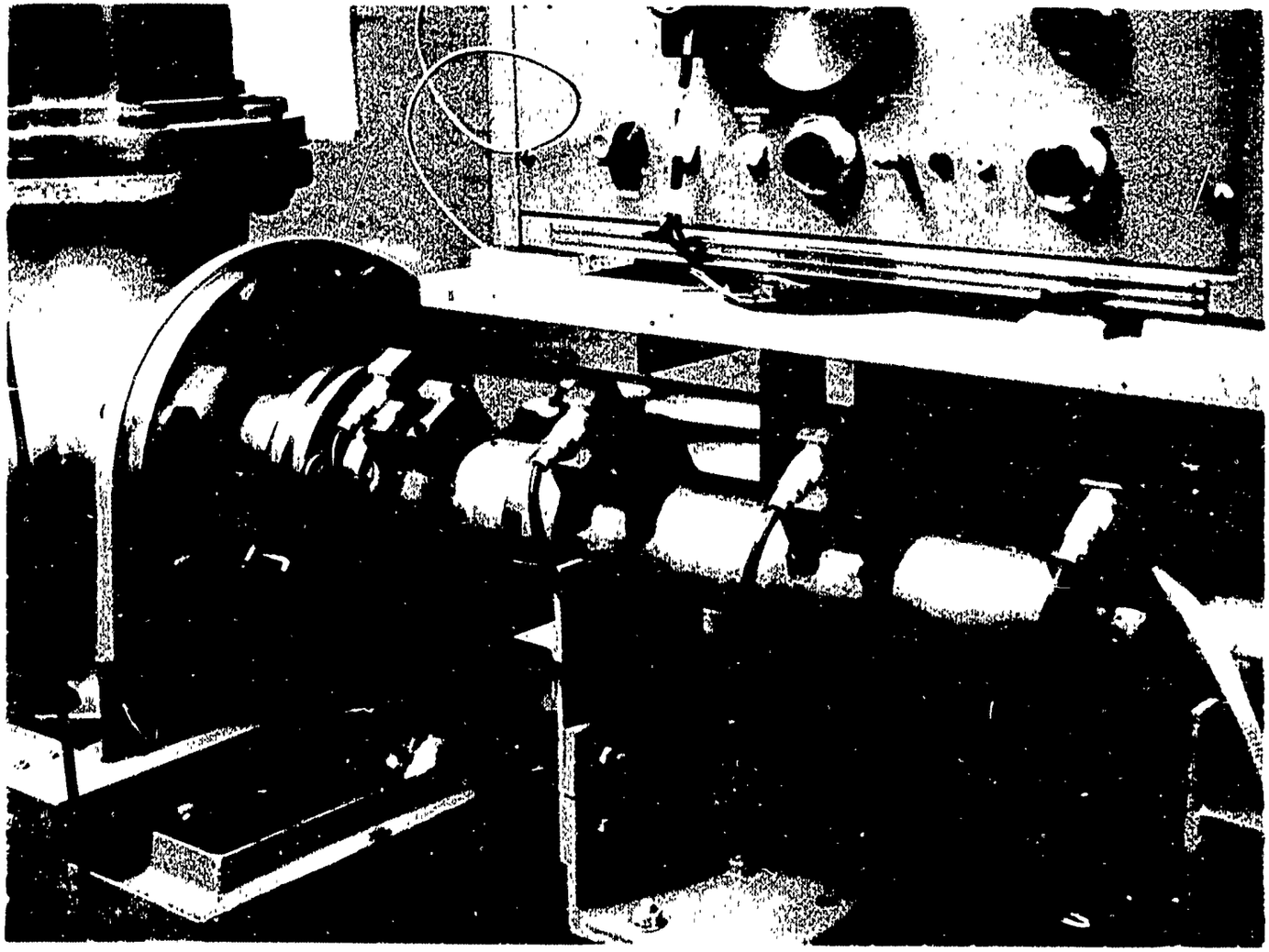

FIG. 2.4 SHOCK VELOCITY MEASURING STATIONS AND COUPLER TO HIGH VACUUM SYSTEM

a) View from Shock Tube Side

b) View from Mass Filter Side

FIG. 2.5 END FLANGE OF SHOCK TUBE SHOWING CONICAL LEAK INSERT AND THIN-FIIM GAUGE INSERT

A scribing technique was developed because it was found that one could significantly reduce the bursting pressure of the heavier diaphragm materials. It also promoted petaling of the diaphragm upon rupture and thus minimized the amount of diaphragm material that was carried down the shock-tube during each shock; since aluminum diaphragms were used, this feature meant that the tube itself has to be cleaned infrequently.

The scribing tool appears in Figure 2.6. It consists of a scribe with a tungsten carbide cutting tip mounted in a yoke that can swivel vertically in a block. At the cutting end of the scribe there is located a weight cup to which weights can be added to vary the depth of the scribe mark in the diaphragm material.

The following procedure is used in preparing a diaphragm for the shock tube. Blanks of aluminum foil to 0.005 inches thick, which have been previously cut to fit the shock tube, are placed on a surface plate and the center of the diaphragm is located. With a straight edge, two guide lines are penciled perpendicular to one another, each passing through the center of the diaphragm. Using a straight-edge to steady the cutting tip of the scribe, one scribes marks in the diaphragm along the guide lines by pulling on the block of the scribing tool. This is illustrated in Figure 2.7. The length of the scribe mark is three inches, the same as the shock tube inside diameter. With practice the diaphragms can be made to burst very reproducibly.

To test reproducibility, a batch of ten diaphragms were made up according to the above procedure. During the tests, argon was used as the test gas at the same initial pressure for each shock. Helium was used in the driver section and the diaphragms were burst by allowing the pressure

in the driver section to build up slowly. From the results of the ten tests it was found that the shock velocity was reproduced to 1 per cent.

Since the bursting pressure is constant for a fixed scribing technique, the shock strength is changed by varying the composition of the driver gas. By variation of mixtures of argon and helium from pure argon to pure helium, the entire range of desired shock strengths is obtained. A typical bursting pressure is 1100 mm Hg. with 5 mm Hg. test gas pressure.

2.3 GAS MIXING APPARATUS AND SHOCK TUBE VACUUM SYSTEM

The gas mixing equipment and the shock tube vacuum equipment are schematically shown in Figure 2.8. The gauges and controls for this system can be seen behind the shock tube in Figure 2.3.

The construction of the system is as follows. Three 2100-cubic-inch oxygen tanks made of 304 stainless steel serve as mixing and storage tanks for the test gases used in the shock tube (Figure 2.9). Each tank is connected to the high vacuum manifold through a one-inch diameter, high conductance, stainless steel bellows-sealed valve (marked A, B, C in Figure 2.8). A 1/4 inch nickel alloy diaphragm sealed valve is also connected to each tank and is used to admit the gases for mixing and storage. This same valve also is used to let gas out of the tanks and into the shock tube. The tanks are wrapped with heating tapes and fiberglass insulation. They are baked out to 250°C for 24 hours before use.

High purity gases from commercial cylinders are admitted to the tanks through three stainless steel valves. The three valves are provided to admit three separate components for mixing. The 1/4-inch stainless steel valves (Robbins Aviation Corporation) have double o-ring stem seals to minimize bursts of air that might be admitted from outside the system.

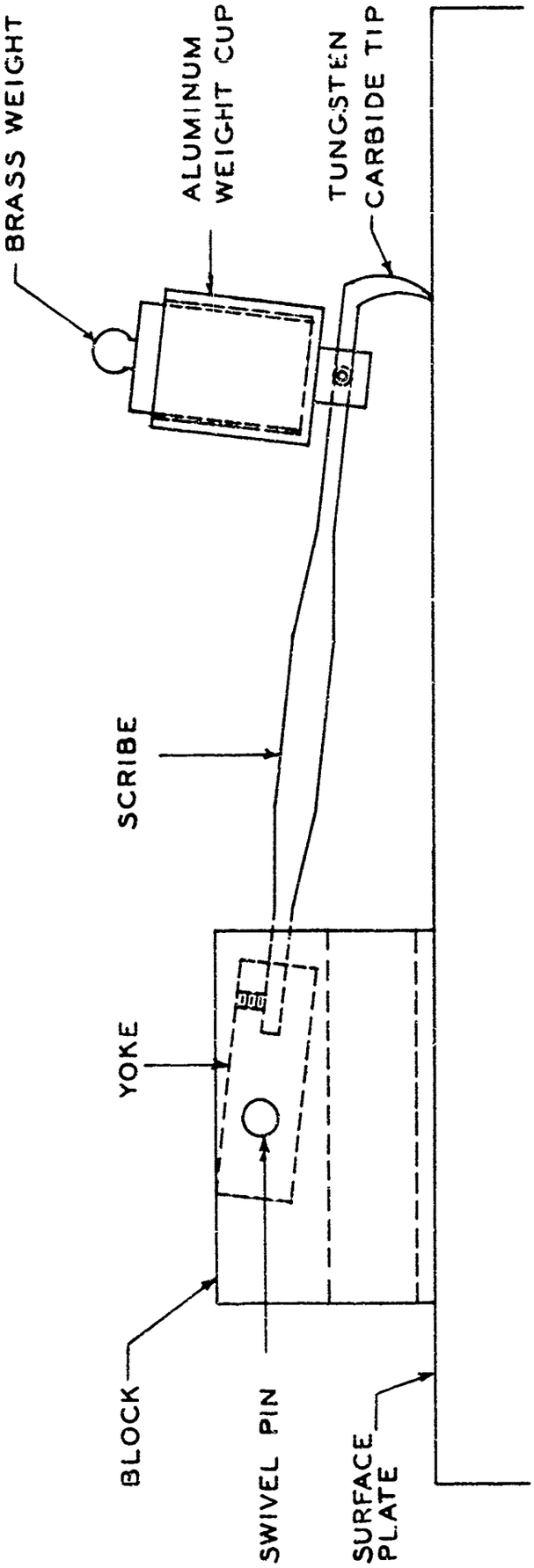

FIG. 2.6 DIAPHRAGM SCRIBING TOOL

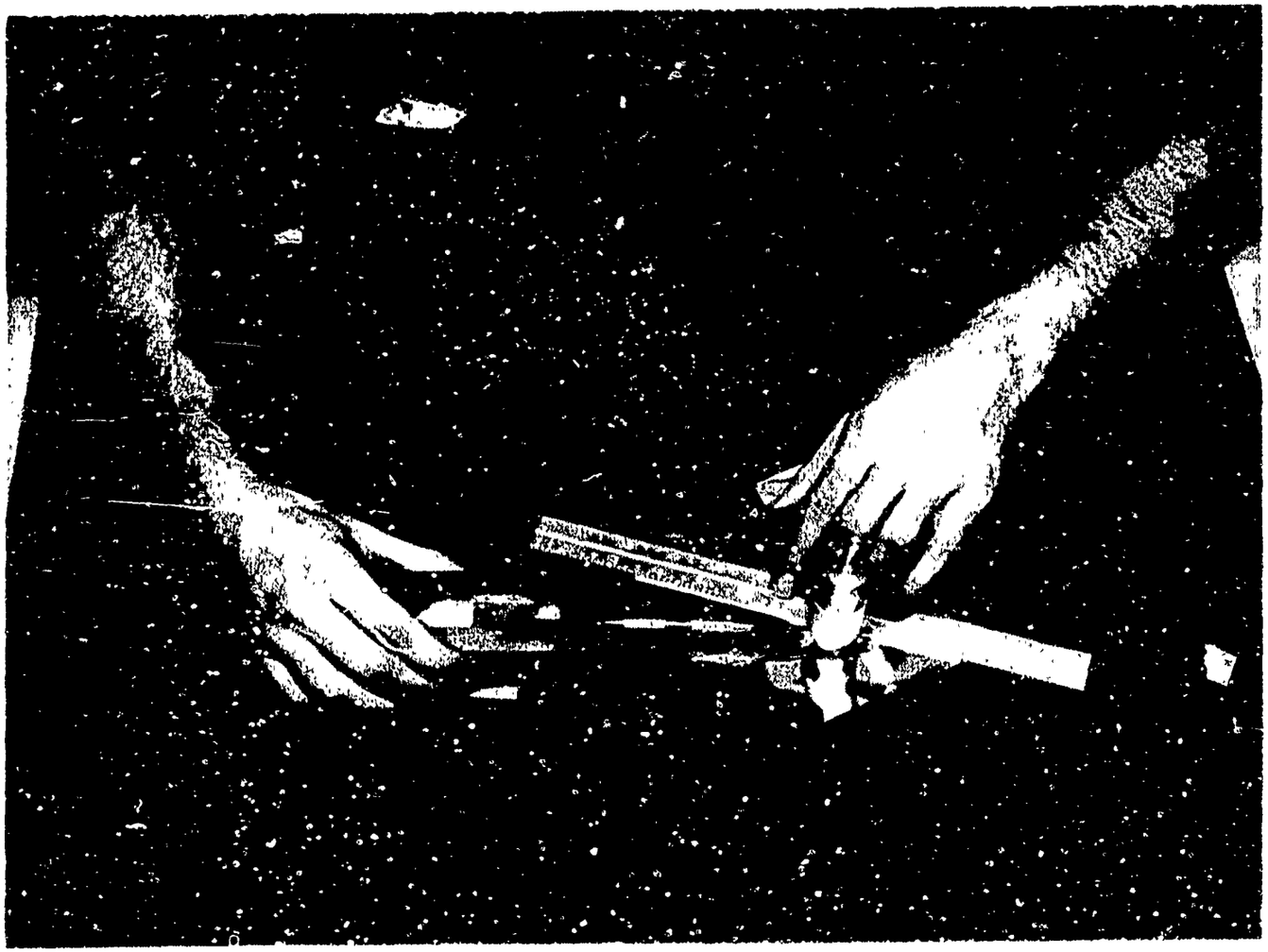

FIG. 2.7 DIAPHRAGM SCRIBING TECHNIQUE

The pressure in the tanks is measured by three Wallace and Tiernan precision differential pressure gauges with 0.3% (of full scale) accuracy. The gauges are used as absolute pressure indicators with their cases evacuated. Their ranges are 0-750 mm Hg., 0-55 mm Hg., and 0-20 mm Hg. That gauge is used which will give at least 50 per cent of full scale deflection when the final pressure is reached. The gauges are so connected that they may also be used to measure the gas pressure in the shock tube. The 0-20 mm Hg. gauge is used because initial shock tube pressures fall in this range.

All the tubing used to connect the gauges, valves, and tanks is 1/4-inch diameter stainless steel seamless tubing. Each connection is made with flared fittings which crush a greaseless teflon o-ring confined in a ferrule (Koncentric flare fittings). The entire gas mixing system is leak-tight as tested with a helium mass spectrometer leak detector.

The high vacuum for the gas mixing apparatus and the shock tube is provided by a liquid-nitrogen-baffled mercury diffusion pump. The pump is connected to a stainless steel manifold from which are valved outlets for the shock tube, the three tanks, the pressure gauges, and all connecting tubing. Normally the tanks and lines are evacuated to below 10^{-6} mm Hg. before use and the shock tube to below 10^{-5} mm Hg. before admitting the gas to be tested.

The driver section of the shock tube is pumped out with only a Duo-Seal rotary pump before driver gases are admitted. Helium and argon are both used. The driver section itself is used as the mixing chamber. The pressure is measured by two Wallace and Tiernan gauges with ranges of 0-400 mm Hg. and 0-3000 mm Hg.

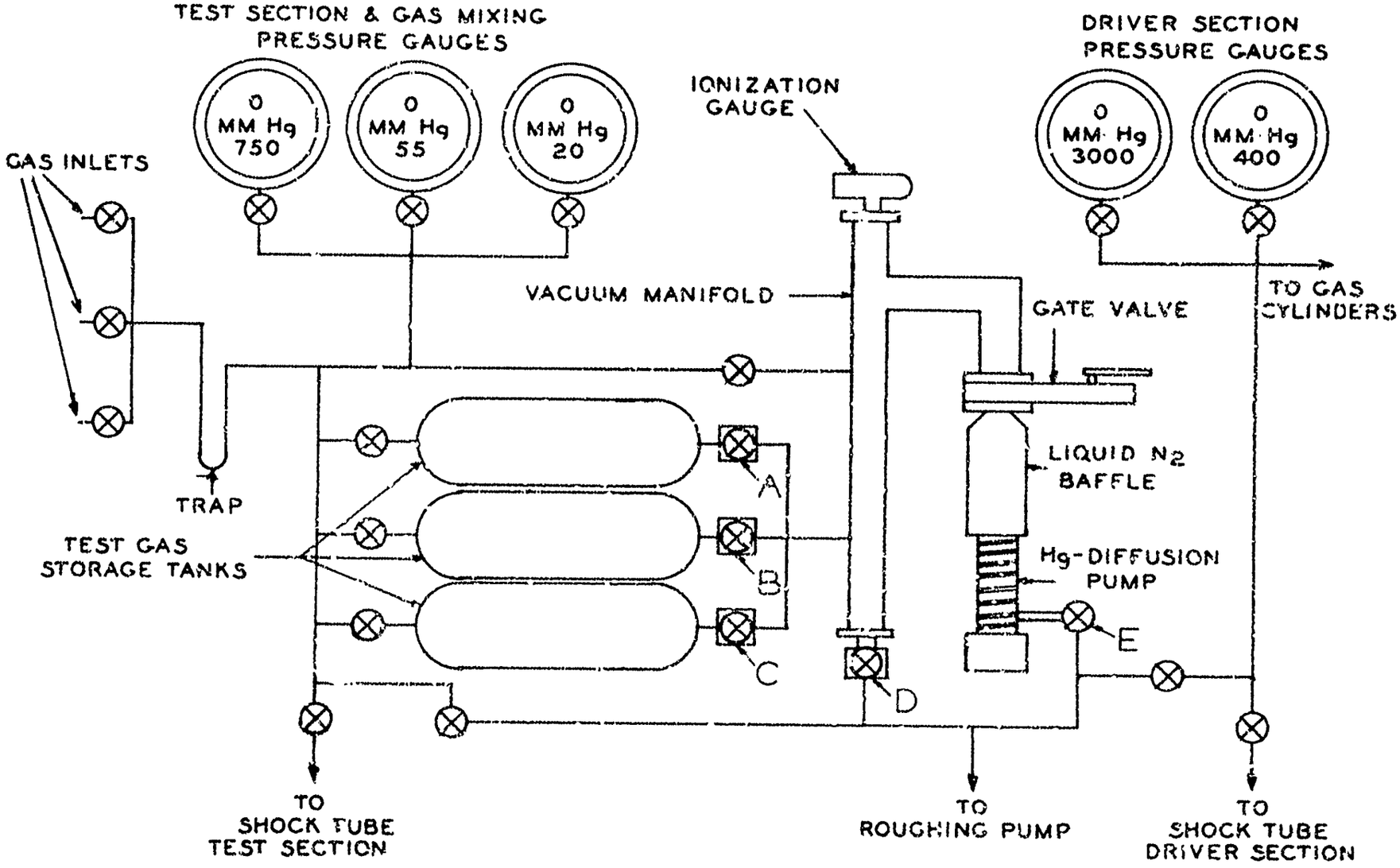

FIG. 2.8 GAS MIXING APPARATUS AND SHOCK TUBE VACUUM SYSTEM

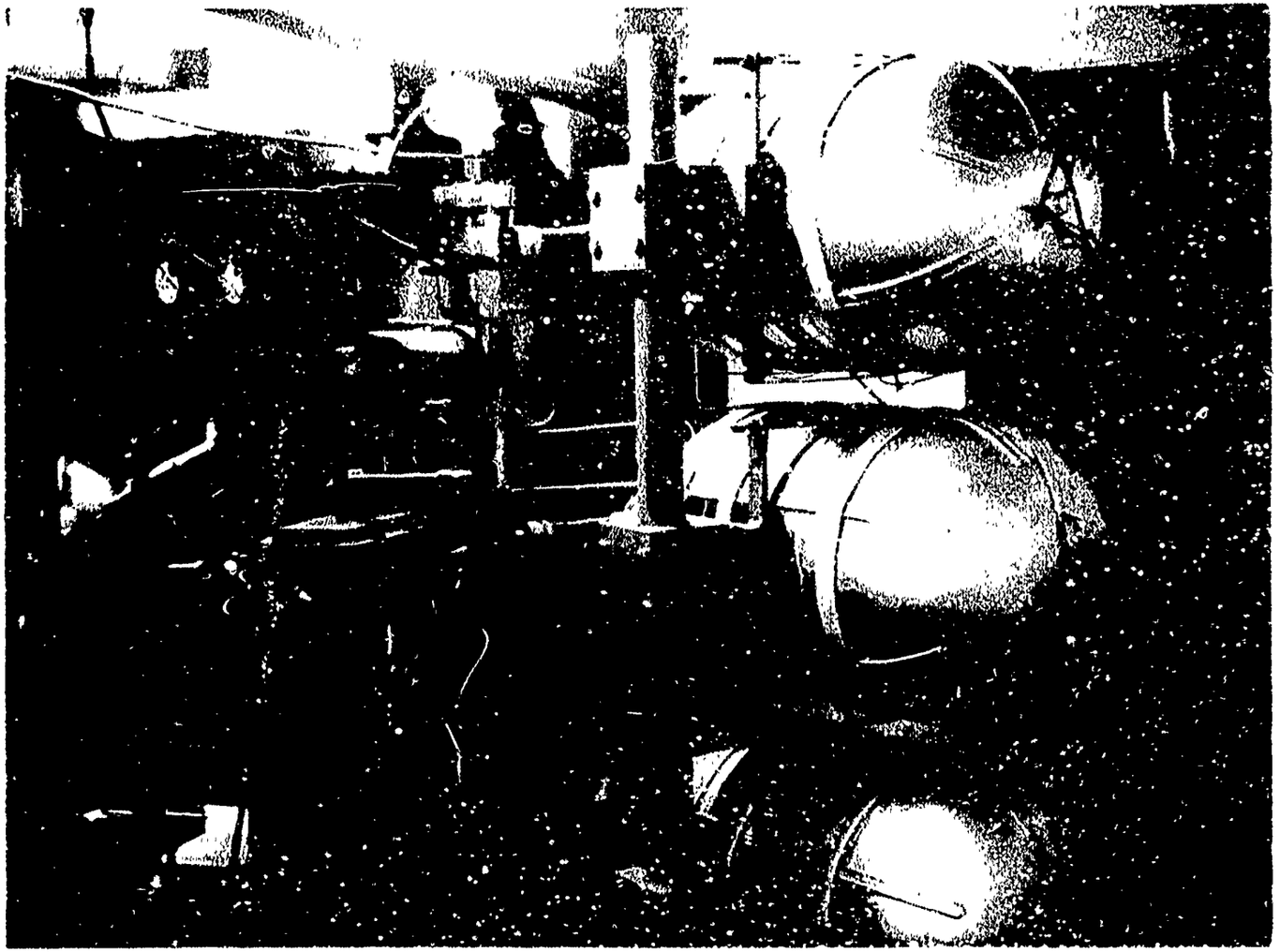

FIG. 2.9 GAS STORAGE TANKS AND HIGH VACUUM MANIFOLD

The normal method of operation is to admit helium gas to a desired pressure and then slowly admit argon until the diaphragm bursts.

2.4 SHOCK VELOCITY MEASUREMENT

The velocity of the shock wave is measured by detecting its passage past four thin-film platinum resistance gauges (Figure 2.4).[42] The four probes are connected in series with a load resistor and battery to provide constant current operation. A current of about 20 milliamperes is usually used. The heating of the thin film by the passing shock front changes its resistance, and the resulting voltage change is amplified and differentiated. (Figure 2.1).

The signal from the first probe triggers a single sweep of a Tektronix 535A oscilloscope fitted with a type CA dual trace input. The subsequent signals are then displayed on top of an unfolding raster time base generated by a Radionics Inc. Model TWM-2A crystal driven triangle wave and time mark generator. This same unit also provides time marks at ten microsecond intervals on the raster pattern by z-axis modulation of the scope beam. The single sweep is photographed with a Tektronix C-12 oscilloscope camera fitted with a polaroid back (Figure 2.1).

The thin-film headers were prepared according to the method employed by Steinberg and Davies.[43] Two-pin hermetically sealed glass-to-metal headers (Electrical Industries Type 50GS/40W-HS-2A) were machined to fit into the probe and then ground and polished flat. With a two-hair camel hair brush, a thin straight line film of Hanovia Bright Platinum No. 5 was painted between the terminals. The films were between 1/4 and 1/2 millimeters wide and 0.21 inches long (the distance between the pins). The headers were then heated slowly in a furnace to 580°C and kept there for

one hour. After cooling, the points where the film contacted the pins in the header were cleaned with a file and then painted with small dots of DuPont No. 5815 Silver Conducting Epoxy. The headers were then reheated to 160°C for one hour to dry and then to 260°C for one hour to cure. The treatment with epoxy was found necessary to reduce electrical noise coming from the junction of the film and header lead. The final resistance of 150 ohms was used in the first position to trigger the oscilloscope sweep.

The headers were then soft-soldered into the probes, which fit into adjustable barrels. This mounting technique not only allowed good flush mountings with the shock tube wall, but also provided the necessary vacuum seals (Figure 2.10).

The probes fit into holes bored into a shock tube section near the end flange. The holes were bored on a mill seven inches apart to an accuracy of ± 0.007 inches.

The signals from the probes could be read off the raster pattern to within 0.5 microseconds. Since a typical time interval between signals is 200 microseconds, the time interval accuracy is 0.25%. The maximum overall error in the measured velocity is then 0.5% as shown below.

$$v = \frac{s}{t}$$

$$\frac{\Delta v}{v} = \frac{\Delta s}{s} + \frac{\Delta t}{t} = \frac{0.014 \text{ inch}}{7 \text{ inch}} + \frac{0.5 \text{ microseconds}}{200 \text{ microseconds}}$$

$$\frac{\Delta v}{v} \cong 0.5\%$$

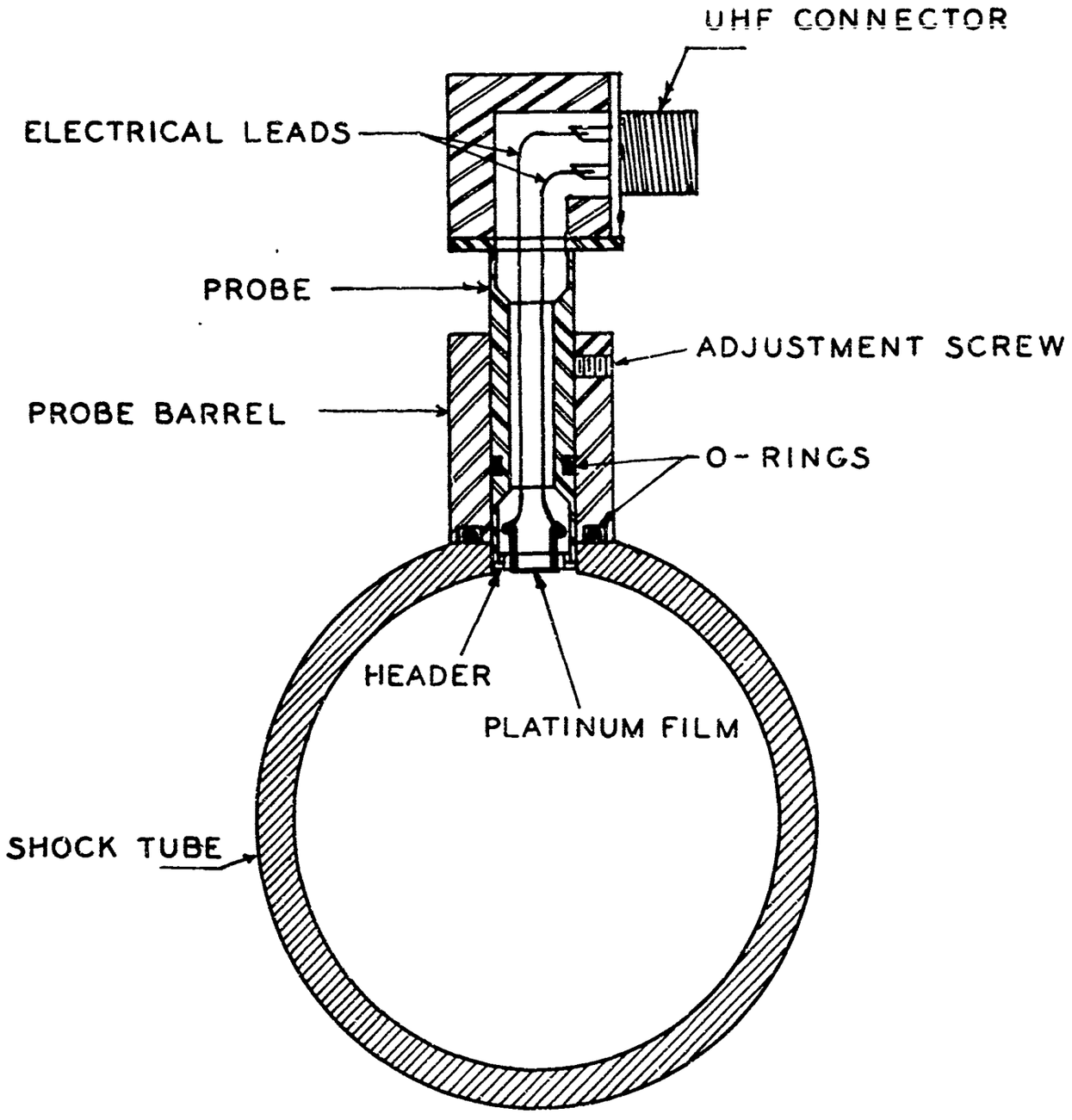

FIG. 2.10 THIN-FILM RESISTANCE GAUGE MOUNTED ON SHOCK TUBE

2.5 THE QUADRUPOLE VACUUM SYSTEM

The vacuum chamber which houses the quadrupole mass-filter and which is coupled to the last section of the shock tube is made from a 150-lb eight-inch-diameter stainless-steel-flanged cross connected to a 150-lb eight-inch-diameter stainless-steel-flanged tee. Between the two is an eight inch gate valve (Figure 2.11, 2.12).

Two six-inch diffusion pumps are used to maintain a high vacuum in the system. An N.R.C. oil diffusion pump and liquid-nitrogen-cooled cryo-baffle are connected to the bottom flange of the tee, and an Edwards mercury diffusion pump is connected to a six-inch gate valve on the bottom flange of the cross. Before gas is admitted into the shock tube, the chamber is pumped down to a pressure below 1×10^{-6} mm. On admission of the gas to be tested into the shock tube, the pressure rises on account of the constant flow of gas from the orifice in the end cap of the shock tube. With both pumps in use, the background pressure can be held below 1×10^{-5} mm with a pressure of 10 mm in the shock tube; i.e., the vacuum chamber pressure is less than one-millionth of the tube pressure.

The last section of the shock tube protrudes into the vacuum chamber through one of the flanges of the cross. A coupler provides the necessary vacuum seal between the shock tube and the chamber. This coupler is so designed that horizontal and vertical adjustment of the vacuum chamber can be done without spoiling the vacuum seal. The adjusting is necessary to accurately align the leak in the shock tube end cap with the ion source of the mass-filter.

The top flange of the cross supports the quadrupole mass-filter. The ion source and ion focusing plates are attached directly to it, and when

the mass-filter is in position the ion source hangs down in the cross directly adjacent the orifice in the shock tube end cap.

An additional vacuum housing also rests on this top flange of the cross. It encloses the quadrupole and its electron multiplier detector. It also contains hermetically-sealed electrical feedthroughs to bring the necessary electrical signals into and out of the vacuum system.

Because the orifice in the end of the shock tube is so small, it was anticipated that it would become frequently blocked with dust or small diaphragm pieces. Therefore, the entire vacuum housing and pumps rest on a roller bearing track mechanism. This allows the chamber to slide back and away from the shock tube. The end cap is then exposed and the necessary maintenance can be performed on the leak. Also, the relative position of the shock tube in the test chamber is restored and the accurate alignment of the leak is maintained when one slides the chamber back into position. This feature has proven to be of extreme value, as it is not rare that maintenance is required several times in one day.

2.6 THE GAS ANALYSIS

The dynamic analysis of the gas effusing from the orifice in the end plate of the shock tube is done with the use of a quadrupole mass filter. Gas emerging from the leak is ionized by electron bombardment. The ions thus formed are drawn upwards through eleven focusing cylinders and into the mass filter. There, only the ions of the desired specific mass (mass/charge) can pass all the way through. The ions exciting the field are deflected onto an electron multiplier, the output of which is recorded on an oscilloscope fitted with a Polaroid camera.

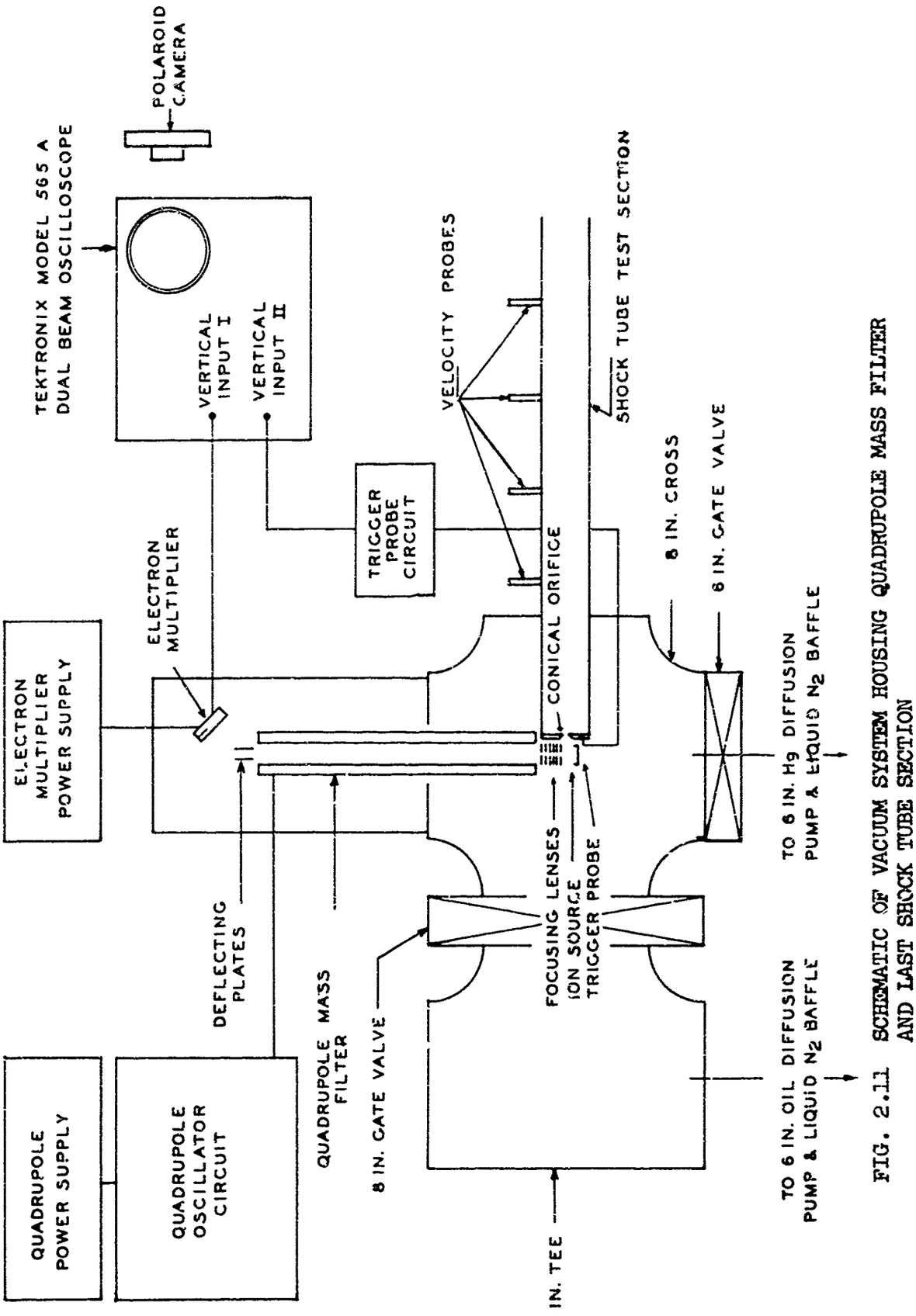

FIG. 2.11 SCHEMATIC OF VACUUM SYSTEM HOUSING QUADRUPOLE MASS FILTER AND LAST SHOCK TUBE SECTION

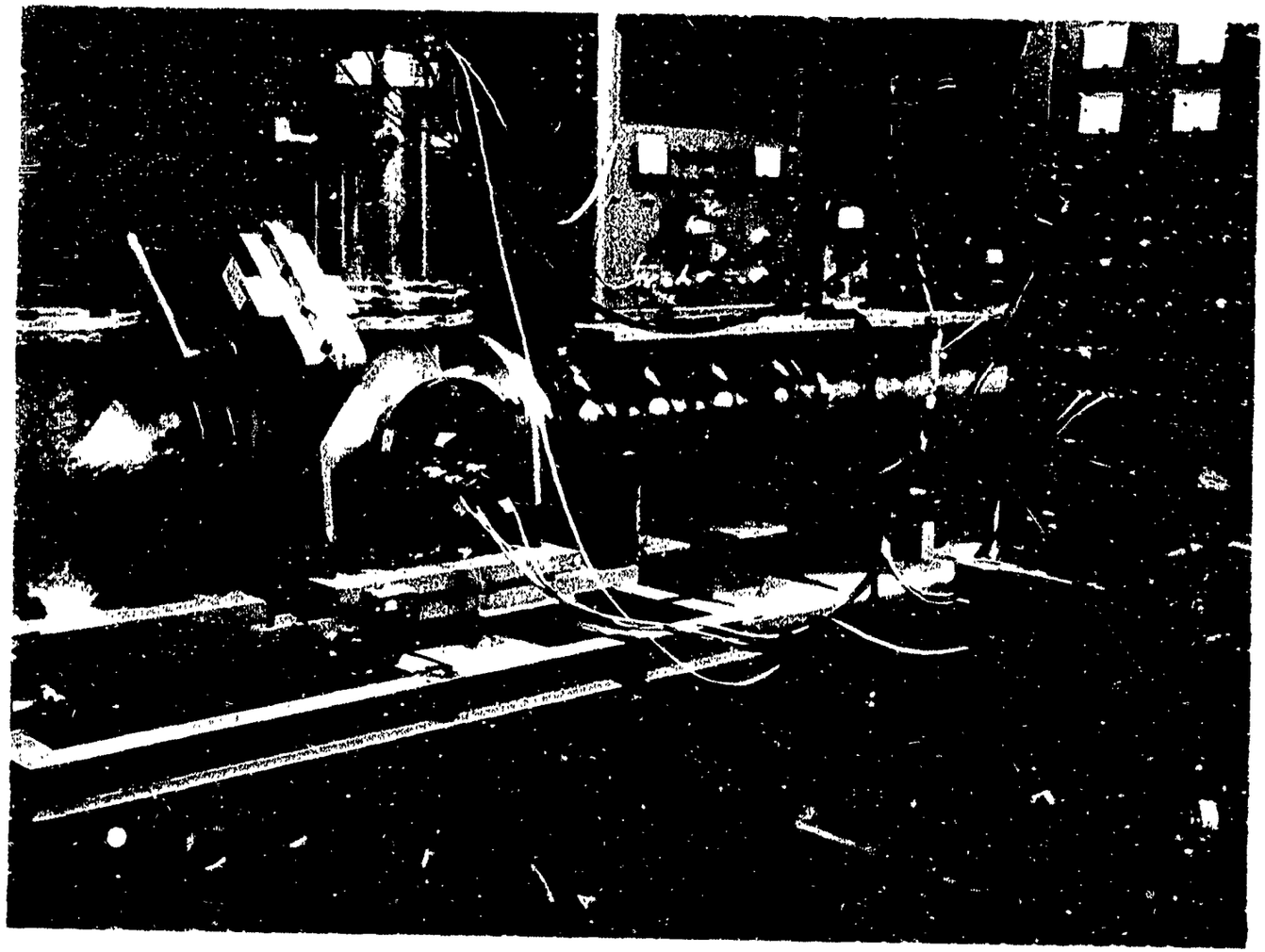

FIG. 2.12 QUADRUPOLE VACUUM SYSTEM AND SHOCK TUBE

2.6.1 THE ION SOURCE

The ion source (see Figure 2.13) consists of an electron beam assembly to ionize the gas and a series of focusing cylinders to move the ions from the ionizing region to the entry hole of the quadrupole mass filter. Most of the metal parts in the ion source are constructed from 0.018-inch Inconel sheet. Where thicker material was needed, 304 stainless steel was used. Several insulating materials were employed. Sapphire rods support and align the ion source, and boron nitride washers hold the focusing cylinders the proper distance apart. Glass bonded mica (Mykroy 1100) is used to make electrical terminal strips and other miscellaneous parts.

Several filament arrangements to supply the necessary electron beams were tried. Since it was not possible to use magnetic collimation of the electrons, the intensity of the electron beam had to be obtained by a filament giving generous emission and a lens system which focused the electrons into the ionizing region. The openings in all the lenses are circular, so it was necessary to use a filament wound in a helix to present the maximum length to the first collimating lens. The filament now being used is made from tungsten wire supported on both ends by tungsten posts. Midway between the posts, the wire is wound in a three-turn helix. This entire assembly is made by Consolidated Electrodynamics Corporation and is the standard filament in their mass spectrometer leak detector (Part No. 38760, Diatron Filament).

The filament is heated with a Sorensen Q Nobatron regulated power supply continuously adjustable from 4.5 to 9 volts. Its maximum output current is 8 amperes. No attempt is made to regulate the filament emission, because the entire recording time of one experiment is less than one

second. Thus, no long term stability is required. About two minutes before a shock is fired, the emission current is checked and is adjusted, if necessary, by changing the filament heating voltage on the power supply. In normal operation the filament is operated at less than two volts so that a series resistance is required with the power supply, which cannot supply less than 4.5 volts. The current required to heat the filament varies between 4.2 and 4.5 amperes.

The electrons emitted from the filament pass through a collimating lens and a focusing cylinder before entering the ionizing region. They exit on the other side of this region and are collected on an electron trap. The collimating lens is connected to the negative side of the filament. The voltage on the focusing lens is supplied by a Kepko ABC 425M continuously adjustable from 0 to 425 volts. The setting used on the focusing lens is determined by monitoring the ion current and using that voltage which corresponds to a maximum. Several lens voltages have been used and they all center around 250 volts.

The voltage on the case determines the final energy of the electrons. This voltage between the filament and the case is supplied by a Kepko ABC 200M regulated power supply adjustable between 0 and 200 volt. This case voltage seems also to have some focusing effect on the electron beam, so it is also adjusted to give the maximum ion signal.

On exiting the ionizing region, the electrons are collected on a plane metal sheet held five volts positive with respect to the case, to suppress secondary electron emission.

The ions formed by the electron bombardment are forced upwards by the ion repeller into the focusing lenses. They enter through a 0.106-inch diameter hole in the top of the case. The center of the electron beam is

0.156 inches below this hole. In order to extract the ions from the case, the ion repeller is made 15 volts positive with respect to the case.

There are eleven cylindrical lenses 0.089 inches in diameter and 0.150 inches long. The cylinders are copper brazed into 0.028-inch thick Inconel plates held apart by boron nitride spacers and supported by sapphire rods. The voltages on all eleven lenses were continuously adjustable from that of the case (75 volts) to ground, the potential of the entry hole into the quadrupole. The geometry of the lens system made the computation of optimum voltages virtually impossible, so that the settings used are those found by maximizing the recorded ion current.

Since this method of focusing ions is highly unconventional, especially in mass spectrometry, the reasons for making the ion optics as they are are listed below.

1. Circular optics instead of slit optics was employed because in a quadrupole mass filter the entry hole is circular.

2. Cylindrical lenses were used because their ends may be placed arbitrarily close together. This was important because the lenses run parallel to the end cap of the shock tube, practically touching it. To prevent the potential of the end cap from penetrating into the lens system, the cylinders were placed 0.007 inches apart.

3. The large number of lenses was necessary because of the long distance the ions had to move. They had to travel two inches to clear the side of the shock tube before entering the mass filter. Also for maximum focusing versatility, the lenses were made only a little longer than their diameter.

4. The diameter of the cylinders (0.089 inches) was a compromise between two desired properties. Their diameters should be large, to admit the largest number of ions from the case, thus increasing the sensitivity. On the other hand, the diameters should be small, to allow the central axis of the cylinders to be as close as possible to the end of the shock tube, which in effect moves the electron beam closer to the leak.

No unique set of voltages was found which gave an absolute maximum ion current. Several different sets which differed markedly from each other all gave approximately the same resultant ion current. However, each set gave a maximum current in the neighborhood of its voltage settings. A typical set of ion source voltages is given in Table 2.1.

The ions enter the mass filter through a final collimating hole. The size of this entry hole has an effect on the resolution of the quadrupole. For this reason it was made adjustable. Several different sized holes were drilled into small metal buttons which can be interchanged in the ion source with relative ease. For any particular experiment, in order to maximize the ion current transmission, the largest hole is used consistent with the resolution required.

2.6.2. THE QUADRUPOLE MASS FILTER

The quadrupole mass filter consists of four round stainless steel rods 0.750 inches in diameter and 17 inches long arranged so that the electric field in the space between them is essentially hyperbolic. The axes of the rods form the edges of a right square prism. The poles are held in place by two stainless steel flanges each fitted with four boron nitride cups to provide electrical insulation, support and location. The flanges

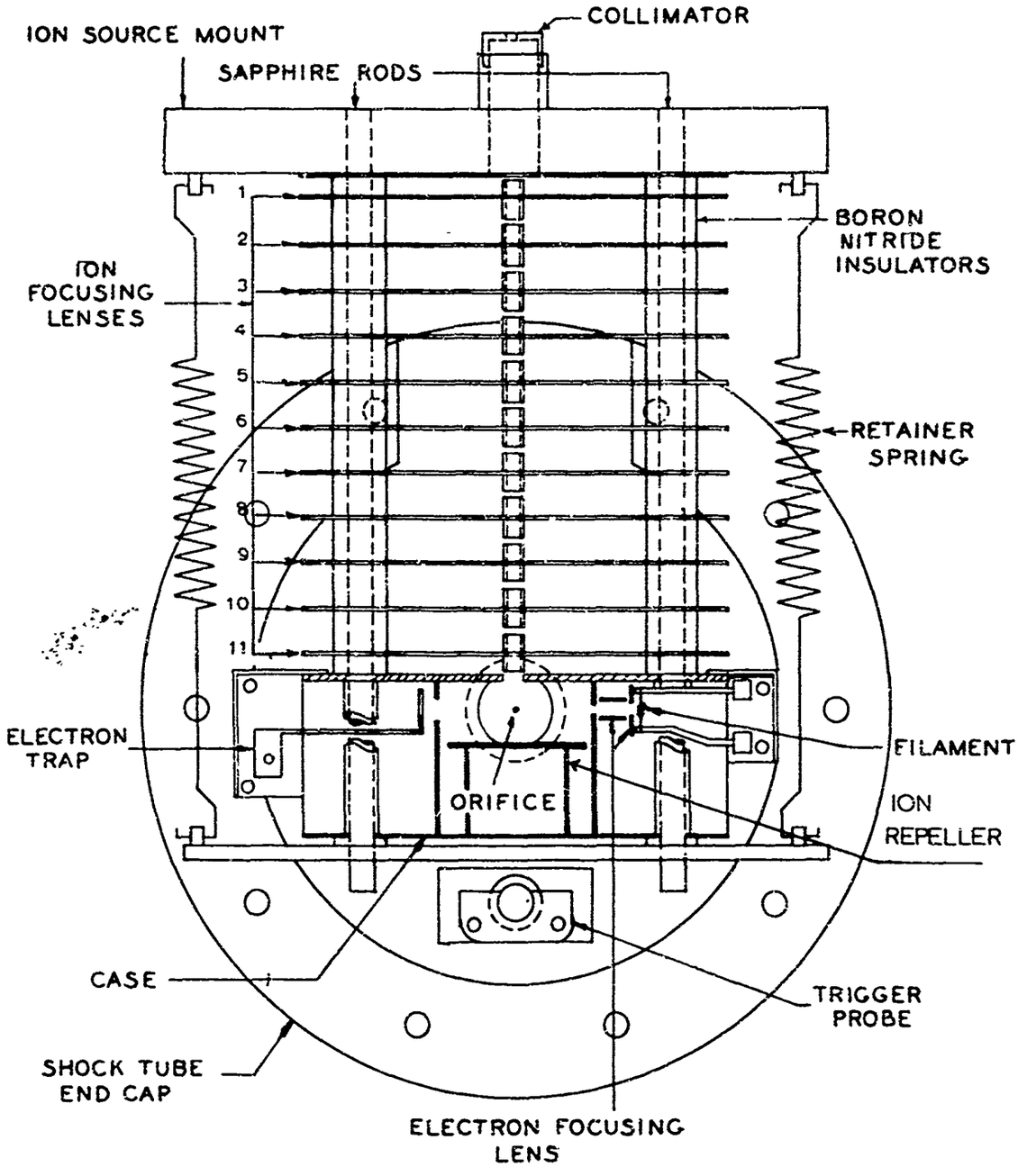

FIG. 2.15 THE ION SOURCE OF THE QUADRUPOLE MASS FILTER AND SHOCK TUBE END SECTION

TABLE 2.1

ION SOURCE VOLTAGES ON QUADRUPOLE MASS-FILTER

ELEMENT	VOLTAGE (VOLTS)
1. Ion Repeller	97.0
2. Case	75.0
3. Ion Focusing lenses	
No. 11	75.0
No. 10	49.3
No. 9	72.8
No. 8	28.7
No. 7	65.2
No. 6	31.1
No. 5	65.4
No. 4	00.0
No. 3	57.9
No. 2	11.7
No. 1	50.4
4. Ion Source Mount	00.0
5. Filament and Flat Electron Lens	-25.0
6. Cylindrical Electron Lens	225.0
7. Electron Trap (trap current 20 microamperes)	70.0

are mutually aligned by bolting them to two ends of a cast stainless steel cylinder. The cylinder has accurately positioned locating holes so that the flanges may be accurately realigned after removal for servicing and cleaning of the rods (Figure 2.14).

The principle of operation is now well-documented and will not be repeated here.[44-46] Opposite poles are electrically connected together and excited with both A. C. and D. C. voltages. An r.f. oscillator circuit supplies a one megacycle signal to the poles such that opposite pairs of poles have signals of the same amplitude but 180° out of phase. The same circuit supplies a positive D. C. voltage to one pair and a negative D. C. voltage to the other pair, also of the same magnitude. The ratio of A. C. to D. C. voltage is externally variable and is adjusted to establish the desired resolution. The mass which is allowed to pass through the filter is controlled by the magnitude of the R. F. voltage. The electrical circuit for the oscillator was supplied by Kent Wilson, University of California, Berkeley. The circuit has since been published.[47]

Typically, the operation of the mass filter is as follows. The oscillator and its power supplies, as well as the ion source, are turned on to warm up for two hours before use. Gas is admitted into the shock tube and an ion signal is recorded by the electron multiplier detector. The output of the detector is amplified by a Keithley 409 Picoammeter, and its output displayed on a strip chart recorder.

The r.f. amplitude is changed until the desired mass peak is found. Then several mass spectra are fun in the region of the desired peak, each time changing the resolution by varying the A.C. to D.C. ratio. The spectra are inspected, and that one with the lowest resolution which still has no interference from neighboring peaks is used. This is done because the

transmission of the ion current decreases as the resolution is made to increase. The optimum r.f. voltage and voltage ratio for the mass being studied are then set and locked. Between runs the r.f. voltage is checked to see if the signal has drifted off the top of the peak. With adequate warm-up the drift is slight.

2.6.3. THE ION DETECTOR

The beam of ions emerging from the mass-filter is bent 45 degrees by a parallel plate deflection lens before striking the dynode strip of a Bendix M-306 Magnetic Electron Multiplier. The output of the multiplier passes through a 10,000 ohm resistor, and the voltage thus generated is amplified by the 2A61 preamplifier of a Tektronix 565 oscilloscope. The preamplifier is used at its one millivolt-per-centimeter setting because the multiplier output cannot greatly exceed 10^{-7} amperes. Higher output currents cause nonlinear gain characteristics.

The Bendix Magnetic Multiplier was employed because it has several advantages over conventional types. Because the active coating on the dynode strip is tin oxide, the entire multiplier can be recycled to moist atmosphere without changing the gain characteristics. Also, the strip can be cleaned easily with a pencil eraser. The oxide coating is also inert to most of the gases being analyzed. Therefore, the gases in the vacuum chamber do not poison the multiplier and change its gain. There is, however, one serious disadvantage to its use. Because the magnetic multiplier has only one dynode, the last stages of amplification cannot be decoupled as in the conventional multi-dynode type. Therefore, the output current must be kept below about 10^{-7} amperes for amplification to remain linear. Since in these experiments essentially D.C. currents are recorded, a very sensitive preamplifier must be used. This sacrifices

bandpass characteristics. The rise time of the 2A61 preamplifier is one microsecond, which is just fast enough for this application.

When this multiplier was first used it lay directly behind the exit hole of the mass-filter and no deflection lens was used. This gave a direct line of sight from the ion source to the detector. With this geometry it was found that the baseline of the mass spectrum never lay at zero ion current. There was always a residual output current on the multiplier, even between mass peaks and when the accelerating voltages were turned off. This last observation was the clue to the fact that the current came from hard ultraviolet or soft x-rays, generated in the ion source, which were reaching the multiplier up the direct line of sight path through the quadrupole mass filter. These higher energy photons also cause secondary emission on the dynode strip and hence would be recorded as ion current. A rough calculation showed that this explanation was reasonable. For this reason the multiplier was set off at an angle and the ion current passed through a lens which deflected it onto the dynode strip. With this arrangement the residual ion current completely disappeared.

The deflection lens voltage is adjustable. This was done for two reasons. Firstly, if the accelerating voltage of the ions is changed, then the deflecting voltage must also be changed to bend the ions through the same angle. Secondly, the high voltage end of the multiplier aids the deflection and thus when the gain of the multiplier is changed by changing this high voltage, an adjustment must also be made on the deflection lens to compensate for this. The lens voltage is supplied by a Kepco ABC 200M power supply. Both positive and negative outputs are connected to ground with 1000 ohm resistors, thus making the voltages on the two plates of the

lens symmetrically positive and negative with respect to ground. The voltage is continuously variable at the power supply and usually is set at about 50 volts.

The output of the multiplier is recorded from the display on the top beam of the Textronix 565 dual beam oscilloscope.

The other beam records the output of the thin-film resistance gauge in the end cap of the shock tube. The schematic of the two inputs into the oscilloscope is shown in Figure 2.11. This thin-film gauge is exactly the same in design as those used for velocity measurement. When the shock wave arrives at the end flange of the tube it heats the gauge, generating a signal which triggers both beams of the 565 oscilloscope preset for single sweep application.

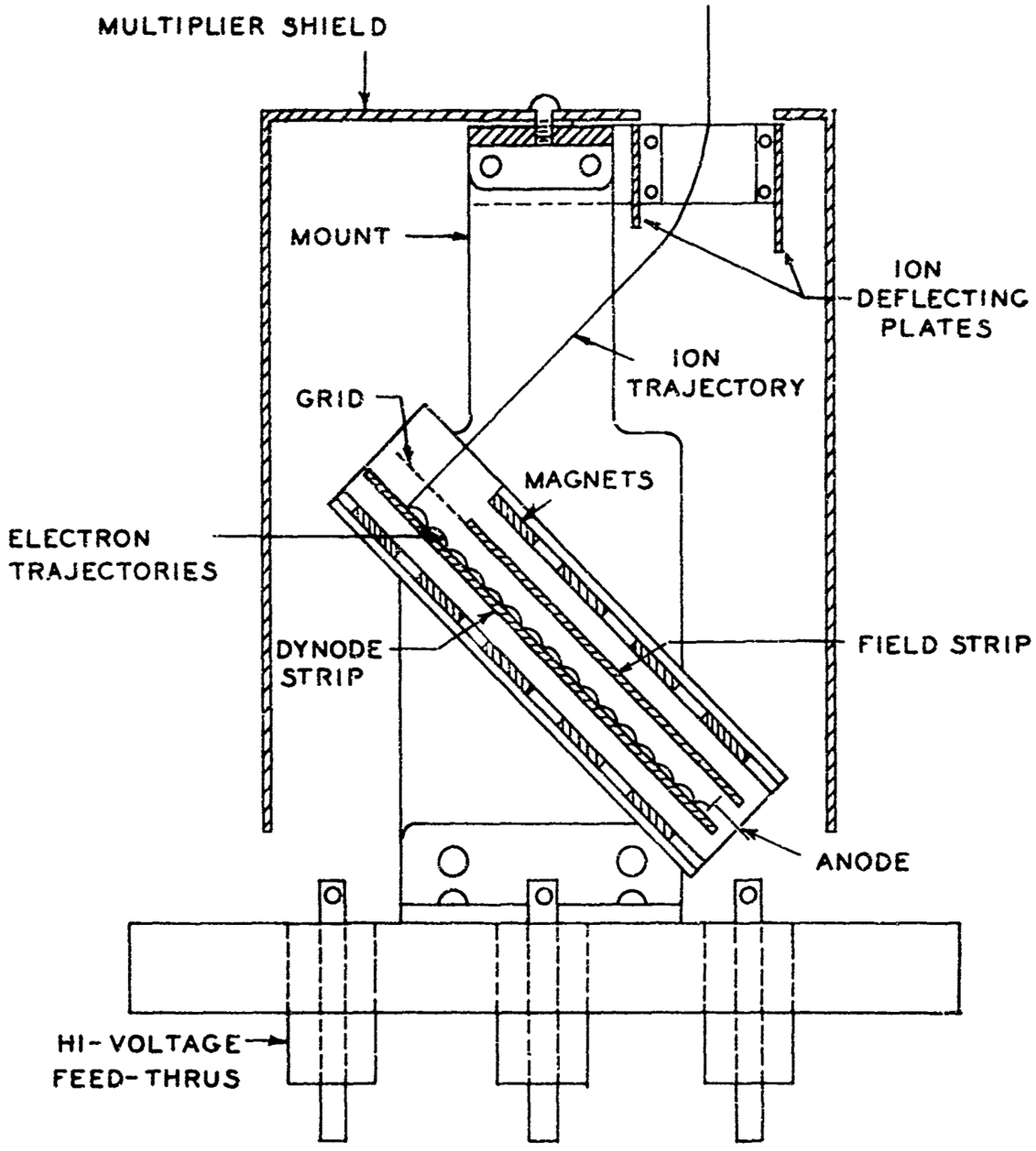

FIG. 2.A ELECTRON MULTIPLIER FOR DETECTING ION CURRENT

FIG. 2.15 ELECTRON MULTIPLIER AND DEFLECTION LENS FOR ION CURRENT DETECTION

3. EXPERIMENTAL

3.1 INTRODUCTION

The results of the experiments performed with the shock tube coupled to the quadrupole mass filter are divided into three sections. The first section covers the results of preliminary tests which were done to calibrate the experimental apparatus. These tests include shocks fired in pure argon, in which the Ar^+ ion current was monitored, and shocks fired in three different mixtures of nitrous oxide highly diluted in argon, in which the N_2O^+ ion current was followed. All these tests were done in order to compare the ion current with the partial pressure of the respective gas in the shock tube.

The second section contains the results of experiments done on the nitrous oxide decomposition reaction. In separate experiments conducted with a mixture of 4 per cent nitrous oxide in argon, the concentrations of N_2O, N_2, O_2, O, and NO were followed as functions of time by monitoring their respective ion currents. In the third section conclusions are drawn with regard to the mechanism of the N_2O decomposition during the testing time of these experiments. Also, data from 38 runs in which the nitrous oxide concentration was followed are reported. They covered a temperature range from 1877°K to 4120°K. The data below 2500°K is correlated with those of others.

3.2 CALIBRATION EXPERIMENTS

Two sets of experiments were done in order to determine the relationship between the ion current of a gas and its partial pressure in the shock

tube. All the tests were run under shock conditions. The first set was a series of shocks fired in pure argon. The purpose was to compare the Ar^+ ion current with the expected total pressure profile in the shock tube. The second set was a series of shocks fired into three separate N_2O^+ Ar mixtures of different N_2O concentrations. The purpose of the second set was to compare the magnitude of the N_2O^+ ion currents with the corresponding partial pressures of N_2O in each of the three mixtures.

3.2.1 CALIBRATION EXPERIMENTS IN PURE ARGON

At the end flange of the shock tube, the pressure of argon as a function of time looks like a step function. Before the shock arrives, the pressure is low and constant. On shock arrival, it rises instantly (less than 5 microseconds) and remains constant until the reflected shock wave interacts with the contact surface and returns to the end wall. This period of constant pressure (and temperature) lasts between 500 microseconds and 2 milliseconds, depending on the final temperature. The highest temperature yields the shortest testing time. Because the temperature is constant, the density also remains constant.

Shocks were fired into pure argon, and the Ar^+ ion currents were recorded. In the earliest experiments, the ion current signals rose very slowly (200-400 microseconds) and did not level off to a constant value. This phenomenon was soon traced to the ionization region (the case), which was too far away from the leak. Thus, the main contribution to the ion current came from the gas pressure building up in the case.

Therefore, a new source was built which was narrower, allowing the electron beam to be placed closer to the leak. The distance of the electron beam from the ion source was originally 25 mm; the new ion source

decreased this distance to 10 mm. The narrower source made the conductance of the case much greater, so that gas from the shock tube which was not ionized could exit more easily into the larger vacuum enclosure. This second source gave faster rises, but even faster results were needed. It was important to have the signal rise in a time which was short compared to the time of a reaction. Therefore, if a reaction should last 500 microseconds, the rise time should be below about 25 microseconds.

At this time we noticed that the electron beam diverged in the case so much that less than one-half of the electron current reached the trap. Since we desired not to use magnetic collimation of the electron beam with the quadrupole mass-filter, it was necessary to insert a cylindrical electrostatic lens in the path of the electrons, in order to focus them onto the trap. At the same time, the case was made a little narrower so that the length of the electron path through the case was reduced. With the electron beam now confined to the center of the case, the ions formed were from the center of the gas beam emerging from the tube. This new arrangement drastically reduced the ion current from the background gas in the case, but still did not give satisfactory rises or levelings in the Ar^+ ion signals.

Up to this point, there had been no ion repeller electrode in the case. The ions were withdrawn by a large negative voltage (with respect to the case) on plate No. 11. The potential on plate 11 penetrated into the source and withdrew the ions. The repeller was omitted in order to have the highest possible conductance through the case. Because of such poor response up to this time, an ion repeller electrode was built into the source.

The addition of the ion repeller immediately gave the desired shape to the argon ion signal and also increased the ion intensity by a factor of at least ten. It was also found that the best signals resulted if plate 11 was operated at the case voltage. This implied that the repeller ejected ions into the mass filter preferentially from the center of the beam, while plate 11 drew out ions preferentially from around the exit hole of the case and not from the beam center.

Two more changes were made before the actual experiments were begun. The electron beam was being deflected by the voltage on the wire connected to the electron lens. The voltage was sometimes as high as 400 volts, which bent the beam completely off the electron trap. Therefore, a screen of nickel mesh (95% transmission) was placed a short distance beyond the exit side of the case. It was close enough to shield the case from stray voltages and far enough back from the case to avoid interference with the free exit of gas.

The source was again brought closer to the leak by making the end flange of the shock tube thinner. The final distance between the leak in the shock tube and the center of the electron beam is 4 mm.

The performance of the source during a shock in pure argon can be gauged by three criteria: (1) the steepness of the rising signal, (2) the squareness of the leveling off to the final value, and (3) the constancy of the final high value. Unfortunately, these three qualities in their best forms are not simultaneously obtainable in the same temperature and pressure range. Our results with regard to these three qualities are tabulated below. The degree of effectiveness of each quality is indicated as follows.

	Initial Pressure	
Final Temperature	Low (2 mm)	High (10 mm)
Low (1800°K)	Steepness worst Squareness worst	Squareness best Leveling best
High (3500°K)	Leveling worst	Steepness best

The results indicate that it is best to operate at high pressures, 10 mm and above. The better performance at higher pressures is probably due to the fact that the flow through the orifice is more definitely in the hydrodynamic region there than at the lower pressures.

Unfortunately, the initial pressure in the shock tube could not be raised higher than the 10 mm mark. Above this pressure, the case pressure was too high to give good results. At pressures above 10 mm, such things as ion current decreasing with increasing pressure began to occur, indicating that the upper limit in case pressure had been reached. Also, the background pressure in the vacuum chamber was at its allowable maximum at a pressure of 10 mm in the shock tube.

Two oscilloscope records of the Ar^{+} ion signal versus time are shown in Figure 3.1. They are not the best obtained, but are somewhat better than average. In both experiments, the initial pressure was 4.7 mm and the initial temperature was 300°K. In Figure 3.1a, the sweep rate is 50 microseconds per cm. The rise is the fastest we have been able to obtain; the square corner is also optimum and the leveling good. The rise time is about 15 microseconds. In Figure 3.1b, the sweep speed is 200 microseconds per cm. This is slow enough to show the falling signal, due to the return of the reflected shock wave from the contact surface. This is also seen on the lower trace, which is the signal from the thin film gauge in the end

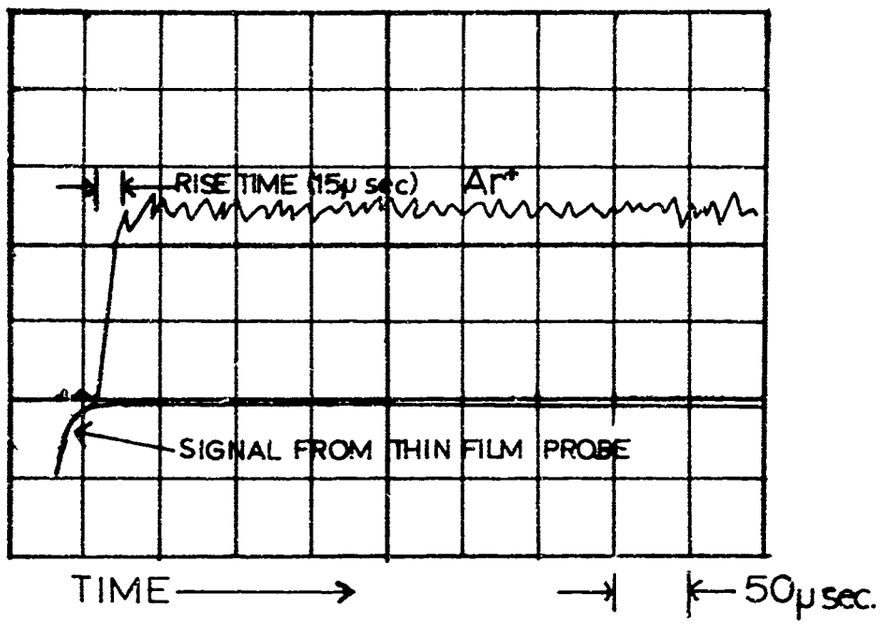

(a.) FAST SCAN

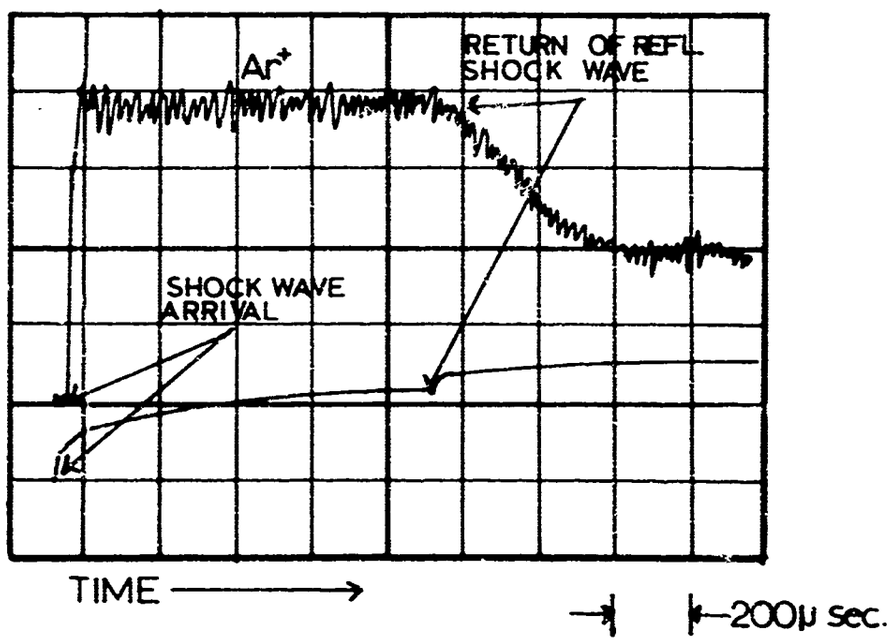

(b) SLOW SCAN

FIG. 3.1 EXPERIMENTAL ARGON ION SIGNAL CURVES

flange of the shock tube. This arrival marks the end of the testing time which, in this case, is 1.0 milliseconds.

3.2.2 CALIBRATION EXPERIMENTS WITH NITROUS OXIDE

Three mixtures, containing 1, 2 and 4 per cent nitrous oxide in argon, were prepared in the gas mixing apparatus.

Several shocks were fired with each mixture, under identical initial conditions. The ion current of N_2O^+ versus time was displayed on the oscilloscope and recorded with a Polaroid camera. The deflection corresponding to the peak N_2O^+ ion signal was measured for each run. This peak occurs just after the steep rise but before reaction causes the signal to fall again. The results showed that the measured ion signal on the Polaroid film was directly proportional to the pressure of N_2O in the shock tube. The results for all runs are tabulated below. In all the runs, the initial pressure was 4.7 mm, the initial temperature was 300°K, and the final temperature was between 2280°K and 2600°K.

TABLE 3.1

PRESSURE DEPENDENCE TESTS

Run Number	N_2O Percentage in Argon	N_2O^+ current (cm deflection)
J28-2	4.0	4.2
J28-3	4.0	4.1
J28-5	4.0	4.1
J28-11	4.0	4.4
J28-6	2.0	2.1
J28-7	2.0	2.3
J28-8	1.0	1.0
J28-9	1.0	1.4
J28-10	1.0	1.3

The linearity is within 10% above two centimeters. The problem at one centimeter is partially due to the uncertainty in the base line from which the deflections were measured. Due to an annoying 60-cycle noise problem, the base line rose and fell approximately 0.2 centimeters at 60 cycles per second. Depending on where the single sweep began, the baseline could have been anywhere from 0 to 0.2 cm above or below the assumed zero point.

In general, however, the experiments were arranged to give initial deflections of over four centimeters, and no data was used after the signal had decayed below one centimeter.

Thus, the experimental apparatus in the final form gave ion signals which were linear with the corresponding density of the species in the shock tube. The linearity is within ±5%.

3.3 THE THERMAL DECOMPOSITION OF NITROUS OXIDE

The experiments on the thermal decomposition of nitrous oxide are divided between those to establish the mechanism and those to determine the rate constant for the disappearance of nitrous oxide.

3.3.1 THE MECHANISM OF NITROUS OXIDE DECOMPOSITION

A large number of runs were made in which the ion currents of N_2O, NO, N_2, O_2, or O were monitored. Particular problems arose with regard to each ionic species. These problems are mentioned below.

N_2O^+

The decay of the N_2O^+ ion current as a function of time was plotted on semi-log paper. The curve was always nearly a straight line (see Figure 3.2). At higher temperatures, however, the curve tended to drop more

slowly than the straight line. We interpret this as due to cooling of the gas at the end flange, where the gas is sampled, with subsequent slowing of the reaction rate. This effect was slight below 2500°K and considerable above 3500°K. In all cases, a first order rate constant (k_1') was calculated for each 100 microseconds of the reaction; then, the constant for the time the reaction began (shock arrival) was found by extrapolation. The procedure for calculating the constant k_1' for Run No. F206513 is shown in Figure 3.2. At 2500°K the extrapolation rarely increased the rate constant by more than 20 per cent from its value at 100 microseconds. At 3500°K the extrapolation increased k_1' by about 50 per cent.

NO^+

The ion current of NO^+ comes not only from the nitric oxide but also from the nitrous oxide. Thus, the initial ion current at shock arrival is exclusively due to nitrous oxide. Data from another run in which N_2O^+ was monitored at the same temperature is used to subtract the N_2O contribution from the NO^+ ion current.

N_2^+

The ion current of N_2^+ also has a contribution caused by the cracking of N_2O in the ion source. A similar subtraction procedure yields the N_2^+ current caused by N_2 in the shock tube.

O_2^+

The ion current of O_2^+ comes exclusively from O_2. Therefore, it gives the most useful (cleanest) kinetic pictures of the course of the reaction. Hence, a large number of runs were made in which O_2^+ was observed.

$\underline{O^+}$

The ion current of O^+ has contributions from N_2O at the beginning of the reaction and NO at the end of the reaction. Since the O atom concentration was always low, no useful information came from monitoring O^+. The only observation made monitoring O^+ was the fact that O atoms did not build up in concentration to a value high enough to be seen on top of the NO contribution to the O^+ peak.

The results at all temperatures are similar, so sample curves are presented at only one temperature--2515°K (see Figure 3.3). In Figure 3.3a the ion currents are plotted, and in Figure 3.3b the ion currents are plotted with subtractions made for the contributions due to N_2O.

The following characteristics were common to all runs:

1. After all the N_2O had decomposed, the O_2^+, NO^+, and N_2^+ ion currents flattened out and remained level.
2. The O_2^+ current rose with a positive curvature for only the first twenty microseconds and then continued to rise to its final value with a negative curvature.
3. Over the entire temperature range of 1800-3500°K, the ratio of NO^+ to O_2^+ after all the N_2O had disappeared was 2.2 ± 0.4.

3.3.2 THE RATE OF N_2O DECOMPOSITION

The rate of disappearance of N_2O was measured in the temperature range 1877°-4120°K. The data from 41 runs made with a 4% N_2O mixture (diluted with argon) are given in Table 3.2. The last three runs (indicated in Table 3.2 with asterisks) were discarded because the amount of decomposition was so slight that an accurate rate constant could not be

TABLE 3.2

EXPERIMENTAL DATA ON 41 SHOCK TUBE EXPERIMENTS
DONE WITH 4 PER CENT N_2O IN ARGON

RUN NO.	SHOCK VELOCITY mm/μsec	MACH NUMBER	REFLECTED SHOCK TEMP. °K	REFLECTED SHOCK DENSITY moles/cc x 10^{-6}	k_1' cc/mole sec. x 10^{-8}
F046526	0.918	2.88	1877	1.81	1.32
F046524	0.993	3.12	2163	1.91	6.38
F046525	1.004	3.15	2210	1.91	5.81
F046503	1.010	3.17	2233	1.94	8.25
Fo46502	1.058	3.32	2430	2.03	16.8
F046504	1.074	3.37	2501	2.04	18.25
F046505	1.091	3.42	2571	2.03	28.61
F046523	1.108	3.48	2651	2.08	23.61
F046522	1.104	3.47	2631	2.13	20.24
F046521B	1.151	3.61	2843	2.13	30.11
F046521	1.155	3.62	2862	2.14	31.74
F046522A	1.189	3.73	3026	2.17	44.14
F046521A	1.252	3.93	3332	2.24	63.23
F206515	0.946	2.97	1976	1.84	2.38
F206514	1.055	3.31	2416	2.03	23.19
F206513	1.081	3.39	2528	2.06	21.86
F206512	1.019	3.20	2266	1.98	11.14
F206510	0.972	3.05	2079	1.89	6.32
F20659	0.966	3.03	2055	1.88	3.25
F20654	1.00	3.14	2186	1.89	10.30

TABLE 3.2 (continued)

RUN NO.	SHOCK VELOCITY mm/μsec	MACH NUMBER	REFLECTED SHOCK TEMP. °K	REFLECTED SHOCK DENSITY mole/cc x 10^{-6}	k_1' cc/mole sec. x 10^{-8}
F266508	1.016	3.19	2256	0.81	14.69
F266511	1.022	3.21	2280	0.86	11.20
F266512	1.068	3.35	2472	0.85	20.05
F266513	1.140	3.58	2792	0.88	35.59
F266514	1.170	3.67	2933	0.94	71.06
F266515	1.091	3.43	2571	0.85	25.66
F266516	1.201	3.77	3083	0.96	62.63
F266517	1.248	3.92	3310	0.98	59.20
F266518	1.257	3.95	3356	0.96	75.88
F266519	1.270	3.99	3421	0.90	104.80
F266520	1.400	4.40	4120	0.99	363.80
F266522	1.140	3.57	2792	4.53	33.06
F266523	1.091	3.43	2571	4.35	18.37
F266523A	1.058	3.32	2430	4.30	14.39
F266524	1.040	3.26	2355	4.25	16.26
F266525	0.951	2.99	1999	3.95	3.79
F266526	1.022	3.21	2280	4.15	8.67
F266527	1.034	3.25	2327	4.22	16.86
*F20657	0.931	2.92	1919	1.89	3.83
*F266506	0.943	2.96	1966	9.78	6.78
*F266521	0.961	3.02	2036	4.00	5.72

*See p. 58.

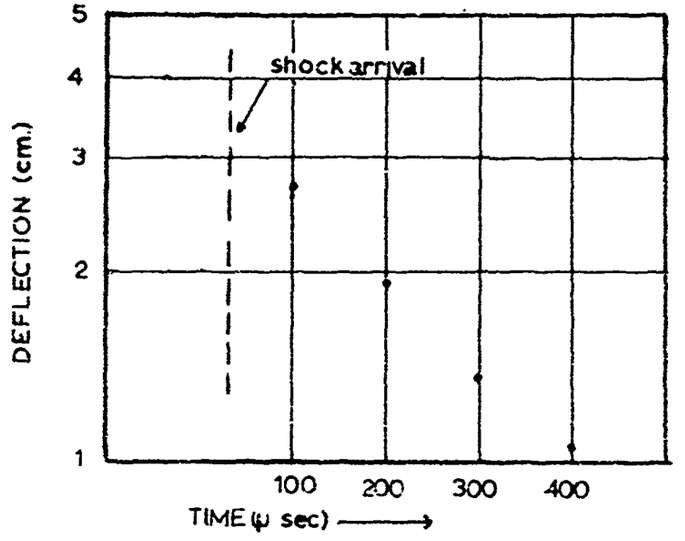

TIME (μsec)	DEFLECTION (centimeters)
100	2.7
200	1.9
300	1.35
400	1.05

(a.) DEFLECTION VS. TIME FOR N_2O DECOMPOSITION

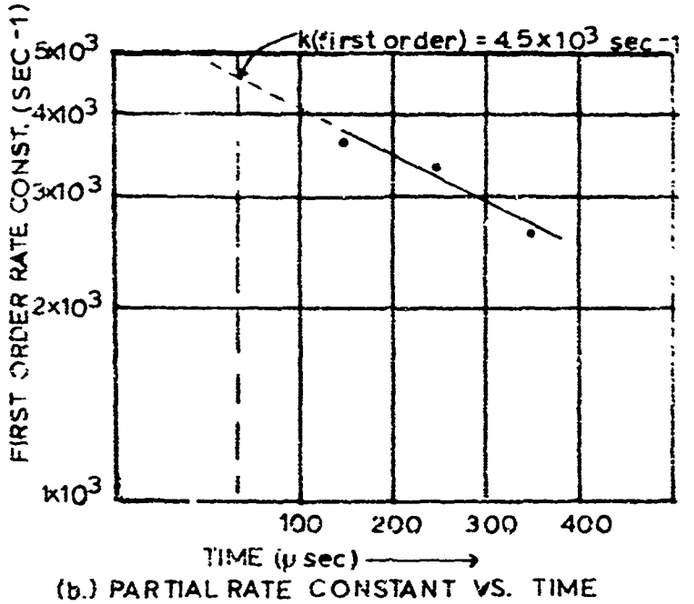

(b.) PARTIAL RATE CONSTANT VS. TIME

FIG. 3.2 . SAMPLE OF PLOTS FOR CALCULATING PSEUDO FIRST ORDER DECOMPOSITION RATE CONSTANT OF H_2O. RUN NO. F206513, T = 2520°K.

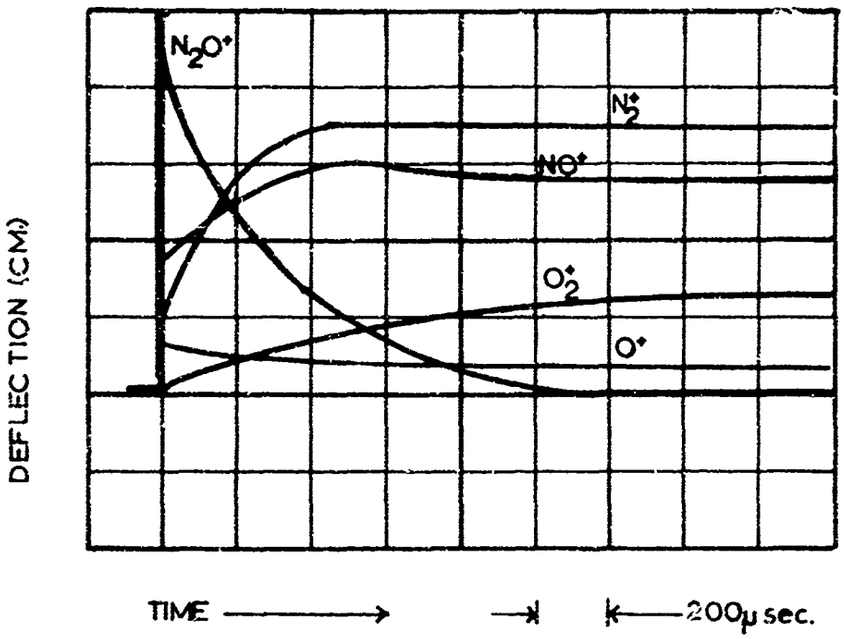

(a) EXPERIMENTAL ION CURRENTS

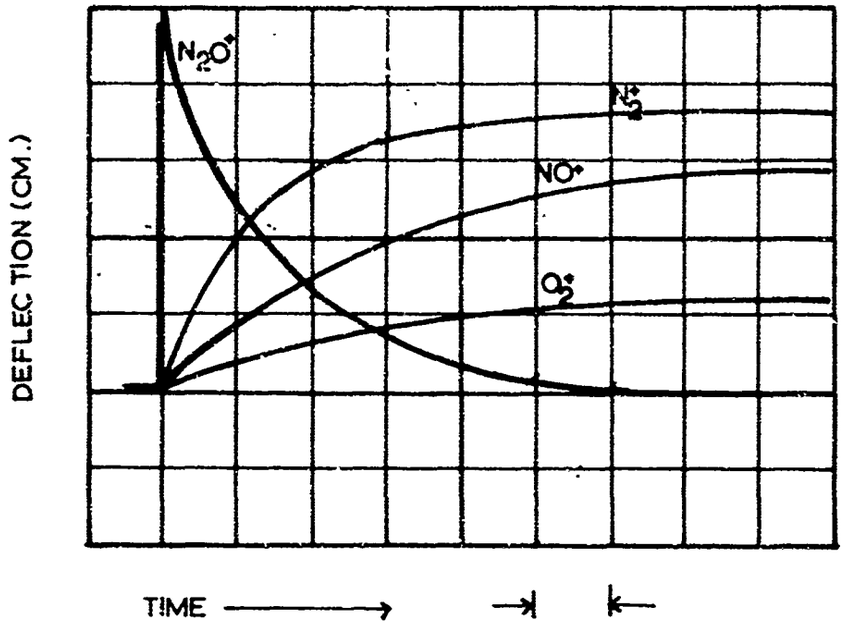

(b) CORRECTED ION CURRENTS

FIG. 5.3 ION CURRENT CURVES IN NITROUS OXIDE DECOMPOSITION REACTION

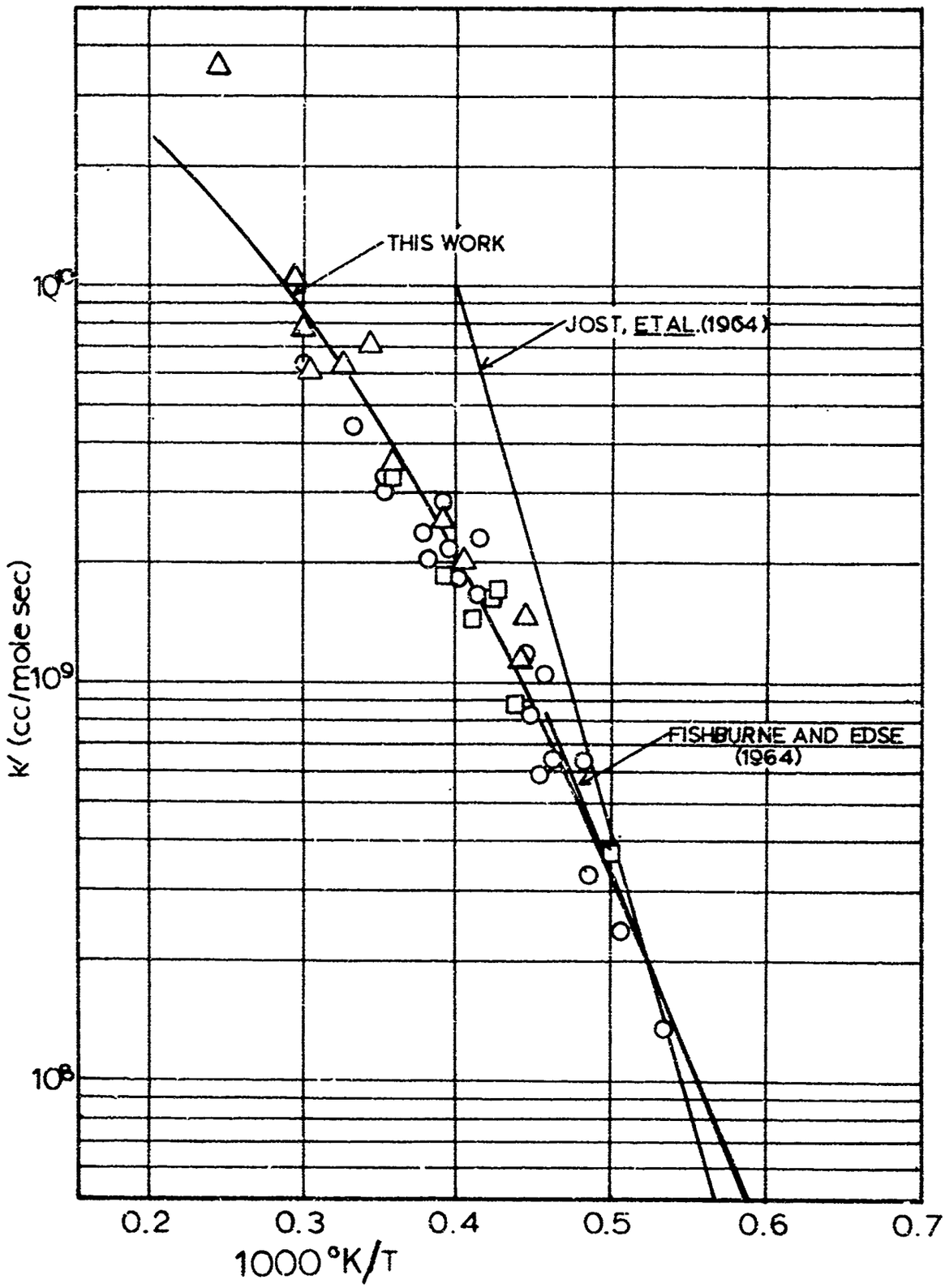

FIG. 3.4 THERMAL DECOMPOSITION RATE OF H_2O (ALL EXPERIMENTS)

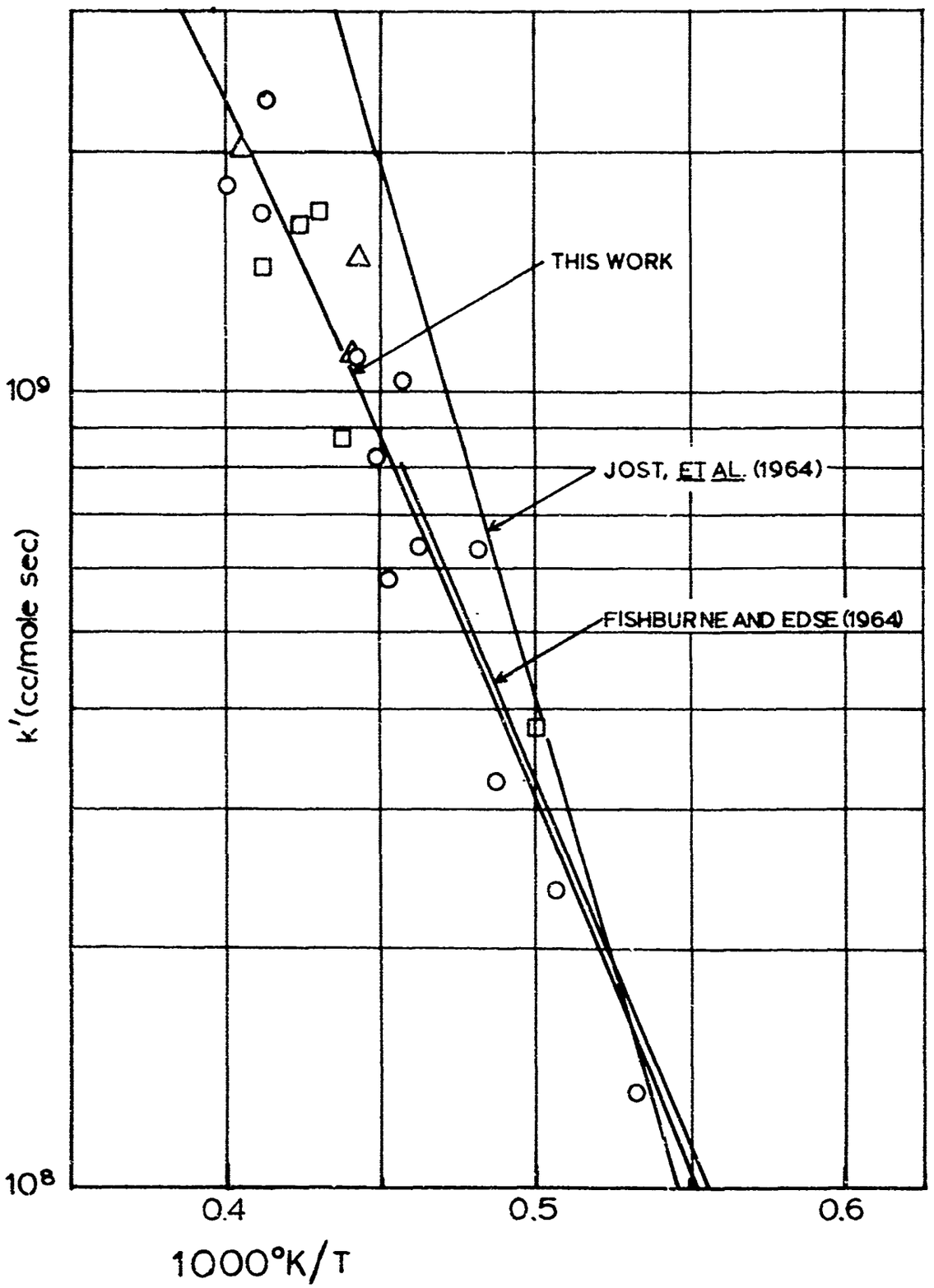

FIG 3.5 THERMAL DECOMPOSITION RATE OF H_2O
(ALL REACTANTS HEATED TO 1000°K)

determined. These runs were not included in the determination of the curves which pass through the data points. A later inspection showed that these three points lay very close to the curves and hence would not have changed the final result had they been included.

The results are plotted in Figures 3.4 and 3.5. The symbols refer to the final gas densities.

Symbol	Final Density
Triangle	0.9×10^{-6} moles/cc
Circle	2.0×10^{-6} moles/cc
Square	4.2×10^{-6} moles/cc

Figure 3.4 shows all thirty-eight points, and Figure 3.5 shows only the points below 2500°K.

Each rate constant was calculated by the following method (see Figure 3.2). From the oscilloscope picture, the deflections at 100 microsecond intervals were measured. (The interval was shorter on the hotter runs.) Then a first order rate constant was calculated for each 100 microsecond interval. (The reaction is pseudo first order because the concentration of argon is constant.) These partial rate constants were then plotted on semi-log paper and extrapolated to the time of shock arrival.

Since the kinetics is second order, the second order constant was calculated by dividing the extrapolated first order constant by the total gas density (essentially the argon concentration).

3.4 CONCLUSIONS

3.4.1 THE MECHANISM OF THE THERMAL DECOMPOSITION OF NITROUS OXIDE

The mechanism of the decomposition of N_2O in the temperature range 1500°-2500°K consists only of the reactions listed below.

(1a,b) $$M + N_2O \underset{k_{-1}}{\overset{k_1}{\rightleftharpoons}} N_2O^* + M$$

(1c) $$N_2O^* \xrightarrow{k_u} N_2 + O$$

(2) $$O + N_2O \xrightarrow{k_2} N_2 + O_2$$

(3) $$O + N_2O \xrightarrow{k_3} 2NO$$

The reasons for this conclusion are listed below.

1. If $k_2 = k_3$ (see Section 3.3.3), then the overall reaction can be written

$$2M + 4N_2O = 3N_2 + 2NO + O_2 + 2M$$

This would predict that the proportionality of the initial concentration of N_2O to the final concentrations of N_2, NO, and O_2 would be $N_2O:N_2:NO:O_2 = 4:3:2:1$. It was determined in a set of experiments at 2515°K (see Figure 3.3) that the ion current proportionality is $N_2O^+:N_2^+:NO^+:O_2^+ = 5.0:3.5:2.8:1.1$; or normalized to $O_2 = 1$, yields 4.5:3.2:2.5:1. The somewhat high value for N_2O could come from the fact that N_2O has a slightly higher ionization cross-section than N_2 or O_2.[48] This is subject to test. The tests are planned for a later series of experiments. The NO value is rather high and may be due to k_3 being slightly

higher than k_2. (In Section 3.3.3 the conclusion is that $k_3/k_2 = 1.2 \pm .2$.) This same semi-quantitative proportionality exists at all temperatures below 2500°K.

2. Jost, et al,[40] in their recent study of N_2O decomposition, found a final NO concentration, after all the N_2O had decomposed, which was consistent with the assumption that 25% ± 5% of the original N_2O reacted to form NO. This yield was independent of temperature. They were unable to follow the O_2 concentration (they used an ultraviolet absorption technique) and hence were unable to draw any conclusions concerning the constants k_2 and k_3. Our hypothesis that steps 1-3 constitute the entire mechanism and that $k_2 \approx k_3$ explains their findings perfectly.

3. The yield of NO and O_2 after all the N_2O decomposed was always the same. The ratio of final yields, $(NO)_f/(O_2)_f = 2 \pm 0.4$, occurred not only in the temperature range 1500°-2500°K, but also at temperatures as high as 3500°K. We have been unable to think of any other set of reactions dealing with the chemical species of this system which could produce this result.

3.4.2 THE STEADY STATE FOR OXYGEN ATOMS

The second conclusion reached is that below 2500°K there exists a steady state concentration of oxygen atoms. The following reasons are offered.

1. The O_2^+ curves rise initially with a positive curvature. After a very brief period (30-50 microseconds), the O_2^+ curves start to rise to their final value with a negative curvature. The initial

rise period never exceeds the time necessary for 10 per cent of the N_2O to decompose, and usually is under 5 per cent. Using these experimental results we have calculated that at the inflection point the O atom concentration is already between 80-90 per cent (or more) of its steady state value. Therefore, the time necessary to reach the inflection point is almost the time needed to reach the steady state concentration of O atoms.

2. The shape of the N_2O^+ curves is essentially first order. If there is deviation from the steady state, the decomposition should accelerate from the first order speed as the O atom concentration builds up. This observation was also made by Jost et al,[40] who also observed essentially first order behavior.

3. Using Fenimore and Jones's value for k_3,[34] along with the experimental result that $k_2 = k_3$, we calculated that the steady state exists up to 2500°K. The criterion used for this calculation was that the O atom steady state concentration never exceeds five per cent of the original N_2O concentration. Above 2500°K the steady state does not result using Fenimore's value for k_3. Kaufman, Gerri, and Bowman's value[32] for k_3 is too low by a factor of 100 to give the observed steady state at 2500°K.

3.3.3 THE RATE CONSTANTS k_2 AND k_3

Over the entire range of this investigation the final yield of NO was always 2.4 ± 0.4 times the final yield of O_2. This implies $k_3/k_2 = 1.2 \pm 0.2$. The uncertainty in the value comes from measurements done at each temperature. There is no indication that this

ratio changes with temperature. Therefore, the inaccuracy in the ratio is mostly in the pre-exponential factor; the activation energies for the two rate expressions cannot differ by more than 1 kcal. Kaufman et al[32] give activation energies which are 1 kcal apart.

The observation of constant NO yield with temperature made by Jost et al[40] confirms the conclusion that $E_3 \cong E_2$.

Fenimore and Jones's value for k_3 now seems to be well-established. Assuming that this value is essentially correct, we derive k_2 from the relation $k_3/k_2 = 1.2$

$$k_2 = 0.85 \times 10^{14} e^{-28,000 \text{ cal/RT}} \frac{\text{cc}}{\text{mole sec}}$$

3.4.4 THE RATE CONSTANT k_1

The rate of disappearance of N_2O was measured in the temperature range from 1877° to 4120°K. The rate of disappearance was found to be proportional to the concentration of N_2O and to the total density, where the argon concentration represents the total density. This is justified because the gas mixture was 96% argon. This may be written as

$$-\frac{d(N_2O)}{dt} = k_1'(N_2O)(Ar)$$

A least squares program was used to fit the data points to the rate expression

$$k_1' = AT^{1/2}\left(\frac{E}{RT}\right)^n e^{-E/RT} .$$

An equation of this form was used because its complexity is just sufficient to permit a reasonable empirical representation of the data points and because the exponent (if positive) has physical meaning in the Kassel

theory of unimolecular reactions. E was taken as the high-pressure activation energy of nitrous oxide, 60,000 cal/mole. The program calculated values for A and n.

For all thirty-eight points, the result is

$$k_1' = 3.3 \times 10^6 T^{1/2} \left(\frac{60{,}000 \text{ cal}}{RT}\right)^{5.84} e^{-60{,}000 \text{ cal}/RT} \frac{\text{cc}}{\text{mole sec}}$$

For all the points below 2500°K, the result is

$$k_1' = 2.5 \times 10^7 T^{1/2} \left(\frac{60{,}000 \text{ cal}}{RT}\right)^{5.09} e^{-60{,}000 \text{ cal}/RT} \frac{\text{cc}}{\text{mole sec}}$$

Because each O atom produced in step 1 consumes another N_2O molecule, the value for $k_1 = 1/2k_1'$.

Therefore, for all points

$$k_1 = 1.6 \times 10^6 T^{1/2} \left(\frac{60{,}000 \text{ cal}}{RT}\right)^{5.84} e^{-60{,}000 \text{ cal}/RT} \frac{\text{cc}}{\text{mole sec}}$$

and for those points which lie below 2500°K

$$k_1 = 1.2 \times 10^7 T^{1/2} \left(\frac{60{,}000 \text{ cal}}{RT}\right)^{5.09} e^{-60{,}000 \text{ cal}/RT} \frac{\text{cc}}{\text{mole sec}}$$

The lines corresponding to the appropriate k_1''s are drawn through the data points in Figures 3.3 and 3.4. The corresponding results from Jost *et al*,[40] and Fishburne and Edse[41] are in each drawing. Fishburne and Edse reported first order constants, so that the appropriate constant was divided by the density before it was plotted.

The agreement with Fishburne and Edse is "perfect." Unfortunately, their data only goes up to 2200°K, so that the high temperature data cannot be compared. Fishburne and Edse ignored steps 2 and 3 and called k_1 the rate of N_2O disappearance. Thus, their agreement with this study is perfect (k_1' is plotted) with respect to the rate of disappearance of N_2O. However, there is a difference in their interpretation of k_1.

The comparison with the data of Jost's group is difficult. Their curve rises more steeply than that of this study (see Figure 3.4), but nevertheless agrees at lower temperatures. Their expression for k_1' (they did not ignore steps 2 and 3) is

$$k_1' = 10^{15.3} e^{-\frac{61{,}000 \text{ cal}}{RT}} \frac{\text{cc}}{\text{mole sec}}.$$

Their data points together with the curve for the above expression are shown in Figure 3.6. This plot is taken directly from their article.[40] It is apparent from their data that the above expression for k_1' does represent the dependence of their experimental rate constant with temperature. Therefore, the difference between their rate expression and ours cannot be ascribed to a bad fit of data to an empirical rate expression.

The rate expression of Jost et al has two questionable features.

1. Their value for the activation energy is the same as the value for the high pressure limit, whereas one expects it to drop when going into the low pressure region, especially at high temperature (Fishburne and Edse find E_1 = 49.5 kcal at these densities and temperatures.)

2. The activation energy is so high that the pre-exponential factor is greater than the collision frequency.

In order to have sufficiently high light absorption, Jost et al conducted their experiments at densities between 1 x 10^{-4} and 0.1 x 10^{-4} moles/cc. Johnston has shown that the low pressure limit is at 0.01 x 10^{-4} moles/cc at 888°K.[21] We have calculated, using simple Kassel theory,[50] that the low pressure limit will shift to higher densities with temperature but will shift only to 0.05-0.1 x 10^{-4} moles/sec

at 2000°K. Jost et al present a limited amount of evidence that their kinetic expression is second order. However, a close look at the data reveals that the order could well be lower. More correlation of their data is needed to firmly establish this point. It is possible that their assumption of second order behavior when the reaction is not quite second order could yield the higher activation energy.

Therefore, it must be concluded that Jost's results are not of unquestionable value, if used for a comparison with the results of this study. There are no other studies on record with which to compare the high temperature results.

Because the mechanism is explicit below 2500°K, and because the experimental technique works well below this temperature, the k_1 for the reaction below 2500°K is accepted as correct. The other k_1 may be low by a factor of 2 if there is no steady state, and even lower if there is serious cooling by the end flange. This is, however, the only data above 2500°K, and therefore should be reported.

The exponent n in the rate expression for temperatures below 2500°K is 5.09. This corresponds to six "oscillators" in the elementary Kassel Theory. The nitrous oxide molecule has four vibrations and two rotations so that the "number of oscillators" should be between 4 and 5. This value for n would correspond to a value for n between 3 and 4. Therefore, the experimental value is too high to be explained by Kassel Theory. Such high exponents have been found in other high temperature systems. Davies[51] studied the thermal decomposition of carbon dioxide highly diluted in argon. He found that an exponent n = 4.88 was needed to fit his data to a similar rate expression. His temperature range was 3500°-6000°K.

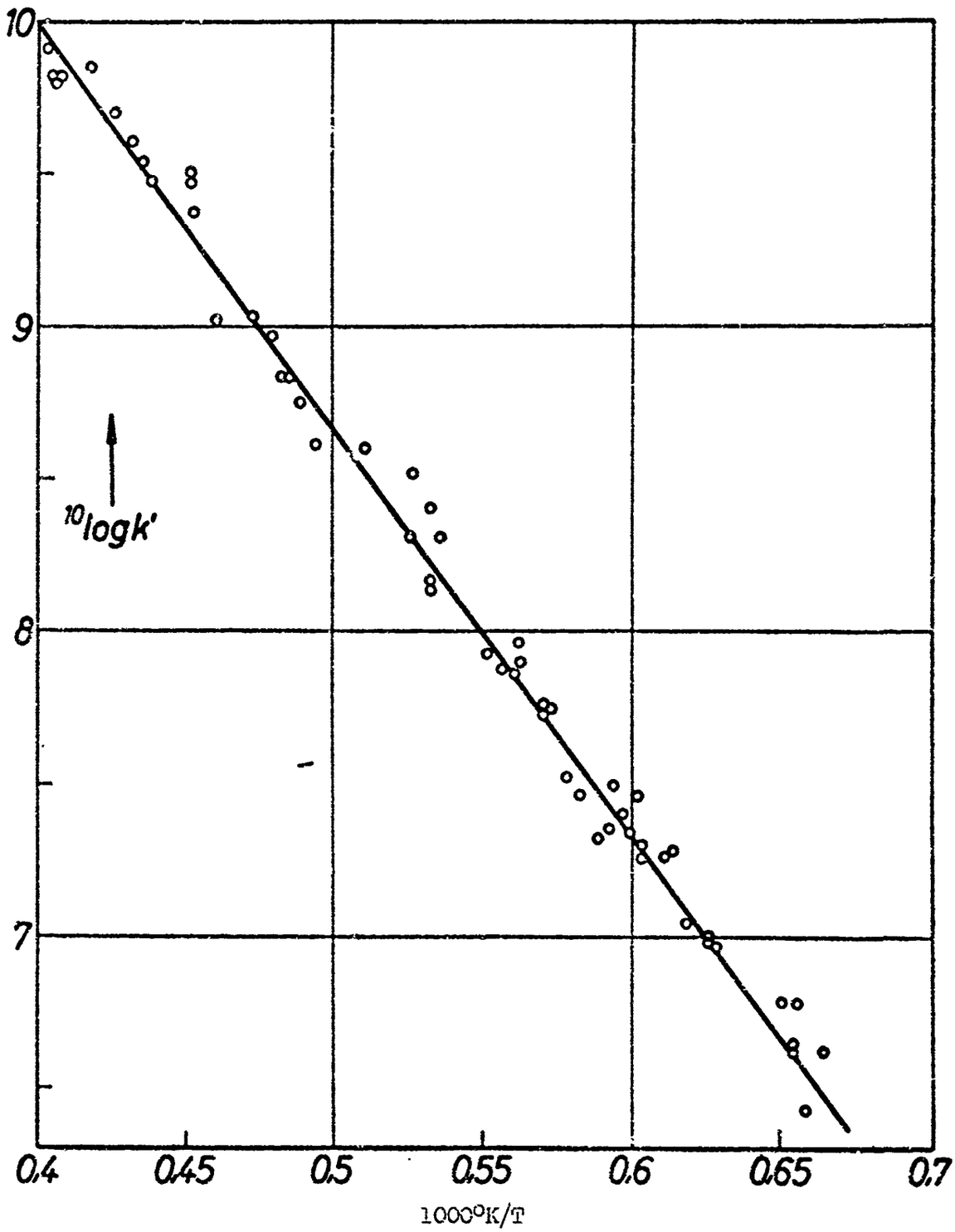

FIG. 3.6 JOST ET AL.'S D.T.A. OF THERMAL DECOMPOSITION OF N_2O.

It is possible that this departure from Kassel Theory is due to a serious departure from a Boltzmann equilibrium distribution among the non-activated molecules. If this were the case, one would expect similar behavior with N_2O at 2500°K to that found with CO_2 at 5000°K, because the activation energy of CO_2 is twice as high (125 kcal/mole for CO_2 against 60 kcal/mole for N_2O). This entire problem will require more investigation for confirmation.

3.4.5 THE REACTION ABOVE 2500°K

Above 2500°K the behavior of this reaction becomes anomalous, and no general conclusion can be made at this time. More experiments need to be done in order to determine the causes of the experimental phenomena found above this temperature. The phenomena observed above this temperature are listed below.

1. In the proportionality of the final concentrations, N_2:NO:O_2, the NO:O_2 ratio remains constant, but the N_2:NO or N_2:O_2 ratio increases. This could be due either to mechanism changes at higher temperature (possibly some chain reaction steps should be included), or to serious departure from the steady state.

2. The O_2^+ curves show shorter and shorter "induction periods"--the time the O_2^+ curve has a positive curvature. This time is about 30-50 microseconds at 2500°K and drops to 5-10 microseconds at 3500°K. This does not necessarily mean that a steady state exists above 2500°K. Since $(^1D)O$ atoms begin to be produced by reaction 1 at high temperatures, they can "instantly" react to form O_2 atoms via the reaction $(^1D)O + N_2O \rightarrow O_2 + N_2$ with probably no activation energy. Thus $(^3P)O$ atoms could be "piling up" between

reactions 1 and 2 or 3, and O_2 could still be produced from the electronically exited (^1D)O atoms. This possibility needs more experimentation for verification.

3. The rate constant for step 1 requires an unusually large "number of oscillators" to account for the apparent falling-off of the rate constant. To fit all the experimental points, the value for k_1 is $k_1 = 1.6 \times 10^{8} T^{1/2} \left(\frac{60{,}000 \text{ cal}}{RT}\right)^{5.84} e^{-60{,}000/RT} \frac{\text{cc}}{\text{mole sec}}$; $s - 1 = 5.8$. [49] Thus, almost seven "oscillators" are needed to fit the data to a classical collision theory expression. When all four vibrations and both rotations (which counts at most as only one vibration) are used, the highest number of "oscillators" is 5. This unusual temperature dependence of the rate constant could be due to any of the facts listed below:

   a. The mechanism of the reaction is changing.

   b. The system is seriously departing from the steady state.

   c. The gas samples from the orifice were cooled by the end flange so seriously that even an extrapolation does not give the correct rate constant.

   d. Simple collision theory is inadequate to explain the high temperature behavior, as demonstrated by Diesen[18] and others in other connections.

BIBLIOGRAPHY

1. J. K. Wright, Shock Tubes (Methuen and Co., London, 1961).

2. J. N. Bradley, Shock Waves in Chemistry and Physics (Wiley and Sons, New York, 1962).

3. A. Ferri (editor), Fundamental Data Obtained from Shock-Tube Experiments (Pergamon Press, London, 1961).

4. A. G. Gaydon and I. R. Hurle, The Shock Tube in High-Temperature Chemical Physics (Reinhold Pub. Corp., New York, 1963).

5. H. O. Pritchard, Quart. Rev. (London) 14, 46 (1960).

6. E. L. Resler, Shao-Chi Lin, A. Kantrowitz, J. Appl. Phys. 23, 1390 (1952).

7. E. F. Greene, J. Am. Chem. Soc. 76, 2127 (1954).

8. D. Britton, N. Davidson, G. Schott, Faraday Soc. Disc., 17, 58 (1954).

9. S. A. Losev, A. I. Osipov, Solviet Physics Uspekhi 4, 525 (1962).

10. Paul F. Bird, R. E. Duff, G. L. Schott, Los Alamos Scientific Laboratory Report LA-2980 (1963), "HUG--A FORTRAN-FAP Code for Computing Normal Shock and Detonation Wave Parameters in Gases."

11. G. B. Skinner, J. Chem. Phys. 31, 268 (1959).

12. G. Rudinger, Phys. Fluids 4, 1463 (1961).

13. C. D. Johnson and D. Britton, J. Chem. Phys. 38, 1455 (1963).

14. J. N. Bradley and G. B. Kistiakowsky, J. Chem. Phys. 35, 256 (1961).

15. J. E. Dove and D. McL. Moulton, Proc. Roy. Soc. (London) A283, 216 (1965).

16. G. T. Skinner, Cornell Aero. Lab. Report No. RM 1396-A-1, (1961).

17. J. N. Bradley and G. B. Kistiakowsky, J. Chem. Phys. 35, 264 (1961).

18. J. N. Bradley, Trans. Faraday Soc. 57, 1750 (1961).

19. R. W. Diesen and W. J. Felmlee, J. Chem. Phys. 39, 2115 (1963).

20. R. W. Diesen, J. Chem. Phys. 39, 2121 (1963).

21. H. S. Johnston, J. Chem. Phys. 19, 663 (1951).

22. H. S. Johnston, J. Chem. Phys. 20, 1103 (1952).

23. L. S. Kassel, J. Chem. Phys. 21, 1093 (1953).

24. H. S. Johnston and J. R. White, J. Chem. Phys. 22, 1969 (1954).

25. E. K. Gill and K. J. Laidler, Can. J. Chem. 36, 1570 (1958).

26. A. E. Stearn and H. J. Eyring, J. Chem. Phys. 3, 778 (1935).

27. N. Nagasako and M. Volmer, Z. Physik. Chem. B10, 414 (1930).

28. Briner, Meiner and Rothen, J. Phys. Chem. 23, 609 (1962).

29. F. F. Musgrave and C. N. Hinshelwood, Proc. Roy. Soc. (London) A135, 23 (1932).

30. R. N. Pease, J. Chem. Phys. 7, 749 (1939).

31. L. Friedman and J. Bigeleisen, J. Am. Chem. Soc. 75, 2215 (1953).

32. F. Kaufman, N. J. Gerri and R. E. Bowman, J. Chem. Phys. 25, 106 (1956).

33. C. P. Fenimore and G. W. Jones, J. Phys. Chem. 62, 178 (1958).

34. C. P. Fenimore and G. W. Jones, 8th (International) Symposium on Combustion (Williams and Wilkins Co., Baltimore, 1962).

35. B. G. Reuben and J. W. Linnett, Trans. Faraday Soc. 55, 1543 (1959).

36. C. P. Fenimore, J. Chem. Phys. 35, 2243 (1961).

37. F. Kaufman and J. Kelso, 7th (International) Symposium on Combustion (Butterworths, London, 1959).

38. G. Porter (Editor), Progress in Reaction Kinetics, Vol. 1, (Pergamon Press, London, 1961).

39. F. Kaufman and J. R. Kelso, J. Chem. Phys. 23, 172 (1955).

40. W. Jost, K. W. Michel, J. Troe, H. Gg. Wagner, Z. Naturforschg. 19a, 59 (1964).

41. E. Stokes Fishburne and R. Edse, J. Chem. Phys. 41, 1297 (1964).

42. V. Blackman, J. Fluid Mech. 1, 61 (1956).

43. M. Steinberg, W. O. Davies, A.R.L. Technical Report 60-312.

44. W. Paul, H. P. Reinhard and U. von Zahn, Zertschrift fur Physik 152, 143 (1958).

45. E. Fischer, Zeitschrift fur Physik 156, 1 (1959).

46. W. Paul, M. Raethes, Zeitschrift fur Physik 140, 262 (1955).

47. K. R. Wilson, University of California Radiation Laboratory Report No. UCRL-11605 (1964).

48. J. W. Otvos and D. P. Stevenson, J. Amer. Chem. Soc. 78, 546 (1956).

49. R. H. Fowler and E. A. Guggenheim, Statistical Thermodynamics (Cambridge University Press, New York, 1952), Chapter 12.

50. S. W. Benson, The Foundations of Chemical Kinetics (McGraw-Hill, New York, 1960, p. 234).

51. W. O. Davies, J. Chem. Phys. 41, 1846 (1964).

VITA

David Gutman was born on November 2, 1934, on the Island of Malta. He immigrated to the United States at the age of three. He attended public schools and graduated from Hilmar Union High School, Hilmar, California, in June, 1952. He attended the University of California at Los Angeles for two years and then enlisted in the United States Army. He served for three years as a medical laboratory technician in an army hospital in Augsburg, Germany. He was honorably discharged in January, 1958, at which time he resumed his studies at the University of California at Berkeley, where he received his Bachelor of Science degree in Chemistry in June, 1960. He entered the Graduate College of the University of Illinois in September, 1960.

UNCLASSIFIED
Security Classification

DOCUMENT CONTROL DATA

(Security classification of title, body of abstract and indexing annotation must be entered when the overall report is classified)

1. ORIGINATING ACTIVITY (Corporate author)

University of Illinois
Department of Chemistry
Urbana, Illinois 61803

2A. REPORT SECURITY CLASSIFICATION
[X] Unclassified
[ ] Other — Specify

2B. GROUP

3. REPORT TITLE

High Temperature Gas Kinetic Study of Nitrous Oxide Decomposition Performed with a Shock Tube and Quadrupole Mass Filter

4. DESCRIPTIVE NOTES (Type of report and inclusive dates)

[X] Scientific Report [ ] Final Report [ ] Journal Article [ ] Proceedings [ ] Book

5. AUTHOR(S) (Last name, first name, initial)

Gutman David
(Belford R L Dr)

6. REPORT DATE AS PRINTED	7A. TOTAL NO. OF PAGES	7B. NO. OF REFS
May 1965	87	51

8A. CONTRACT OR GRANT NO.
AF-AFOSR-588-64

B. PROJECT NO.
9710-03

C. 61445014

D.

9A. ORIGINATOR'S REPORT NUMBER(S) (If given)
Research Report No. 2, Research Group in Shock Tube Kinetics

9B. OTHER REPORT NO.(S) (Any other numbers that may be assigned this report)
AFOSR
AD 66-0952

10. AVAILABILITY/LIMITATION NOTICES

Distribution of this document is unlimited.

[X] Available from DDC
[X] Available from CFSTI
[ ] Available from Source
[ ] Available Commercially

11. SUPPLEMENTARY NOTES (Citation)

Ph.D. Dissertation 1/1/62 - 5/1/65

12. SPONSORING MILITARY ACTIVITY

AF Office of Scientific Research (SRC)
Office of Aerospace Research
Washington, D. C. 20333 Arlington, Va

13. ABSTRACT

A quadrupole mass-filter was built and coupled to a shock tube in order to study high temperature gas kinetics. The chemical kinetics of the decomposition of nitrous oxide was studied with this apparatus in order to establish the mechanis of the reaction at temperatures above 1000°K.

Several instrumentation problems unique to shock tube mass-spectrometry we solved. The most serious problem, that of a rapid-pumping ion source, was overcome by the design and construction of an unusually thin ion source.

The thermal decomposition of nitrous oxide was studied by shock-heating a mixture of 4% N_2O in argon and monitoring the ion currents corresponding to all of the principal species involved in the reaction: N_2O, N_2, O_2, NO, and O. In each run with the shock tube, the mass-filter was tuned to follow the concentration of a single species. Because enough runs were made with all of the species, a run for each species at the same temperature was made for several temperatures. The results of all of the experiments are listed below.

13. ABSTRACT (continued)--

1. The mechanism of the N_2O decomposition between 1500°-2500°K is

(1a,b) $$N_2O + M \underset{k_{-1}}{\overset{k_1}{\rightleftharpoons}} N_2O^* + M$$

(1c) $$N_2O^* \xrightarrow{k_u} N_2 + O$$

(2) $$O + N_2O \xrightarrow{k_2} N_2 + O_2$$

(3) $$O + N_2O \xrightarrow{k_3} 2NO$$

2. $k_3/k_2 = 1.2 \pm 0.2$ for all temperatures between 1500°-2500°K.

3. k_1 the second order rate constant for the thermal decomposition of N_2O in step 1 is equal to

$$k_1 = 1.2 \times 10^{-7}\ T^{1/2} \left(\frac{60{,}000\ \text{cal}}{RT}\right)^{5.09} \left\{e^{-\frac{60{,}000\ \text{cal}}{RT}}\right\} \frac{\text{cc}}{\text{mole sec}}$$

for the temperature range of 1500°-2500°K.

4. The observed steady state for O atoms, as well as the result that $k_3 \approx k_2$, confirms Fenimore's value for k_3 and shows that Kaufman's value for k_3 is inadequate.

14. KEY	LINK A ROLE	LINK A WT	LINK B ROLE	LINK B WT	LINK C ROLE	LINK C WT
Shock Tube	9	3	9	3		
(Quadrupole) Mass Filter	9	3	9	3		
Chemical Kinetics	8	3	8	3		
Thermal Decomposition			8	3		
Mass Spectrometer	9	3				
Argon			5	2		
Nitrous Oxide	8	3	1	3		
Unimolecular Reaction			8	3		
Reaction Mechanism			8	3		
Nitrogen Molecule			1	1		
Oxygen Atom			1	2		
Nitrogen Monoxide (NO)			1	2		
Oxygen Molecule			1	1		

INSTRUCTIONS

1. ORIGINATING ACTIVITY: Enter the name and address of the contractor, subcontractor, grantee, Department of Defense activity or other organization *(corporate author)* issuing the report.

2a. REPORT SECURITY CLASSIFICATION. Enter the overall security classification of the report. Indicate whether "Restricted Data" is included. Marking is to be in accordance with appropriate security regulations.

2b. GROUP. Automatic downgrading is specified in DoD Directive 5200.10 and Armed Forces Industrial Manual. Enter the group number. Also, when applicable, show that optional markings have been used for Group 3 and Group 4 as authorized.

3. REPORT TITLE. Enter the complete report title in all capital letters. Titles in all cases should be unclassified. If a meaningful title cannot be selected without classification, show title classification in all capitals in parenthesis immediately following the title.

4. DESCRIPTIVE NOTES: If appropriate, enter the type of report, e.g., interim, progress, summary, annual, or final. Give the inclusive dates when a specific reporting period is covered.

5. AUTHOR(S): Enter the name(s) of author(s) as shown on or in the report. Enter last name, first name, middle initial. If military, show rank and branch of service. The name of the principal author is an absolute minimum requirement.

6. REPORT DATE: Enter the date of the report as day, month, year or month, year. If more than one date appears on the report, use date of publication.

7a. TOTAL NUMBER OF PAGES. The total page count should follow normal pagination procedures, i.e., enter the number of pages containing information.

7b. NUMBER OF REFERENCES. Enter the total number of references cited in the report.

8a. CONTRACT OR GRANT NUMBER: If appropriate, enter the applicable number of the contract or grant under which the report was written.

8b, 8c, & 8d. PROJECT NUMBER: Enter the appropriate military department identification, such as project number, subproject number, system numbers, task number, etc.

9a. ORIGINATOR'S REPORT NUMBER(S): Enter the official report number by which the document will be identified and controlled by the originating activity. This number must be unique to this report.

9b. OTHER REPORT NUMBER(S): If the report has been assigned any other report numbers *(either by the originator or by the sponsor)*, also enter this number(s).

10. AVAILABILITY/LIMITATION NOTICES: Enter any limitations on further dissemination of the report, other than those imposed by security classification, using standard statements such as:

(1) "Qualified requesters may obtain copies of this report from DDC."

(2) "Foreign announcement and dissemination of this report by DDC is not authorized."

(3) "U. S. Government agencies may obtain copies of this report directly from DDC. Other qualified DDC users shall request through

,,

(4) "U. S. military agencies may obtain copies of this report directly from DDC. Other qualified users shall request through

,,

(5) "All distribution of this report is controlled. Qualified DDC users shall request through

,,

If the report has been furnished to the Office of Technical Services, Department of Commerce, for sale to the public, indicate this fact and enter the price, if known.

11. SUPPLEMENTARY NOTES: Use for additional explanatory notes.

12. SPONSORING MILITARY ACTIVITY: Enter the name of the departmental project office or laboratory sponsoring *(paying for)* the research and development. Include address.

13. ABSTRACT. Enter an abstract giving a brief and factual summary of the document indicative of the report, even though it may also appear elsewhere in the body of the technical report. If additional space is required, a continuation sheet shall be attached.

It is highly desirable that the abstract of classified reports be unclassified. Each paragraph of the abstract shall end with an indication of the military security classification of the information in the paragraph, represented as *(TS)*, *(S)*, *(C)*, or *(U)*.

There is no limitation on the length of the abstract. However, the suggested length is from 150 to 225 words.

14. KEY WORDS. Key words are technically meaningful terms or short phrases that characterize a report and may be used as index entries for cataloging the report. Key words must be selected so that no security classification is required. Identifiers, such as equipment model designation, trade name, military project code name, geographic location, may be used as key words but will be followed by an indication of technical context. The assignment of links, roles, and weights is optional.